Adaptive Integral Extended State Observer-Based Improved Multistep FCS-MPCC for PMSM

Junxiao Wang, *Senior Member, IEEE*, Yibin Liu, Jun Yang, *Fellow, IEEE*, Fengxiang Wang, *Senior Member, IEEE*, and José Rodríguez, *Life Fellow, IEEE*

***Abstract*—In this article, an improved multistep finite control set model predictive current control (FCS-MPCC) based on adaptive integral extended state observer (ESO) is proposed for permanent magnet synchronous motor. The improved multistep FCS-MPCC based on sector is introduced in the current loop. The elements of the voltage vector set are reduced with different sector division method, so it could reduce the computational burden to some extent. Meanwhile, considering that the high gain ESO will obtain faster convergence, better tracking accuracy in theory and the system disturbance rejection can be enhanced, but the noise suppression performance will become poor. Thus, the adaptive extended state observer (AESO) is proposed to balance the disturbance rejection and noise suppression. When system is subject to disturbance, the adaptive gain will increase to enhance the system disturbance rejection and become small to improve the noise suppression in steady state. However, disturbed by time-varying disturbance, the small gain in the steady state will lead to poor steady-state tracking accuracy. To improve the steady-state tracking accuracy, AIESO is proposed by adding the integral term into AESO. Finally, in order to avoid the sector misjudgment caused by parameter mismatch, the strategy based on ESO is used for disturbance compensation. However the selection of inductance is closed related to the estimated burden of the observer. Thus, the inductance parameter estimation method is proposed to update the initial inductance value to reduce the estimated burden, which can help to suppress the parameter mismatches with a smaller estimated burden of the observer. The simulation and experimental results verify the effectiveness of the proposed method.**

***Index Terms*—Adaptive integral extended state observer (AIESO), finite control set model predictive current control (FCS-MPCC), multistep model predictive control, permanent magnet synchronous motor (PMSM), the adaptive extended state observer (AESO).**

Manuscript received 22 December 2022; revised 3 April 2023; accepted 22 May 2023. Date of publication 25 May 2023; date of current version 28 July 2023. This work was supported in part by National Natural Science Foundation (NNSF) of China under Grants 62273306 and 52277070; and in part by the U.K. Engineering and Physical Science Research Council (EPSRC) New Investigator Award under Grant EP/W027283/1. Recommended for publication by Associate Editor N. R. N. Idris. *(Corresponding author: Junxiao Wang.)*

Junxiao Wang and Yibin Liu are with the College of Information Engineering, Zhejiang University of Technology, Hangzhou 310023, China (e-mail: wangjunxiao19860128@126.com; 2112003052@zjut.edu.cn).

Jun Yang is with the Department of Aeronautical and Automotive Engineering, Loughborough University, LE11 3TU Loughborough, U.K. (e-mail: j.yang3@lboro.ac.uk).

Fengxiang Wang is with the National Local Joint Engineering Researching Center for Electrical Drive and Power Electronic, Quanzhou Institute of Equipment Manufacturing, Haixi Institutes, Chinese Academy of Sciences, Jinjiang 362200, China (e-mail: fengxiang.wang@fjirsm.ac.cn).

José Rodríguez is with the Faculty of Engineering, Universidad Andres Bello, Santiago 8370146, Chile (e-mail: jose.rodriguez@unab.cl).

Color versions of one or more figures in this article are available at https://doi.org/10.1109/TPEL.2023.3279856.

Digital Object Identifier 10.1109/TPEL.2023.3279856

I. Introduction

PERMANENT magnet synchronous motor (PMSM) has the advantages of small size, high power density, and high ratio of moment of inertia, which makes it widely applied in industrial robot, electric vehicles, aerospace, and other fields [1], [2], [3], [4]. At present, model predictive control (MPC) has attracted more attention in the field of motion control due to its advantages of simple implementation and easy handling of nonlinearities and multivariable problems [5], [6]. Among them, finite control set MPC (FCS-MPC) does not require modulator, which can directly utilize the discrete characteristics of the converter and the finite switching siginals to manipulate the inverter, delivering faster dynamic performance [7], [8]. Although FCS-MPC has these advantages, it still faces some serious challenges. For example, as the prediction horizon extend, the amount of computation increases exponentially, especially with the application of multilevel converter, the voltage vectors involved in FCS-MPC also increase, which will result in heavy computational burden [9].

Several research works have been carried out to solve the problem of large amount of computation [10], [11], [12], [13], [14], [15], [16], [17], [18], [19]. In [14], a simplified FCS-MPC was proposed to deal with the heavy computational burden problem. Equivalent transformation and sector distribution were adopted to reduce the amount of computation. In [15], a finite control set model torque control based on a deadbeat solution was proposed, it can avoid enumerating all voltage vectors to reduce the amount of calculation to a certain extent. A model predictive control algorithm based on fast vector selection was adopted in [16], which only needs one prediction to obtain the optimal voltage vector, significantly reducing the complexity and computation of the algorithm. In [17] and [18], a multistep MPC method was introduced. The amount of calculation can be reduced and the performance of system can be improved when the predicted step size is equal to two. In [19], a low-cost multistep FCS-MPCC algorithm is presented for PMSM based on a single dc bus current sensor, it can improve the steady-state performance of the system without significantly increasing the computational burden. In this article, in order to further reduce the amount of calculation in [19], it is considered to apply the different sector division method into multistep model predictive current control in this article, which has less computational

burden compared with [19]. In addition, the measurement noise of speed loop was not discussed in [19]. Considering the PI controller used in the speed loop for PMSM, it is difficult to satisfy the tracking performance and disturbance rejection simultaneously. Thus performance tradeoffs often need to be considered when selecting the parameters, which is not conducive to use in high-performance applications. Described in [20], the two degree of freedom structure of ADRC can balance the tracking performance and disturbance rejection performance. The state and disturbance of system can be estimated by using extended state observer (ESO), and the disturbance rejection performance of system can be improved [21], [22], [23], [24].

However, the measured speed will be subject to measurement noise, this will make noise amplified with high gain ESO. Because of this, the ESO gain is usually limited to a certain value to alleviate noise amplification. The conservative design sacrifices the convergence rate of ESO to some extent, and weakens disturbance rejection performance of the system. To solve this problem, an integral ESO was studied in [25]. The integral of measured output was viewed as a new state variable, which can improve noise suppression but result in the increase of the ESO order. In [26], a method to extend the filter equation into ESO was proposed. The disturbance estimation and noise suppression are considered simultaneously. Although noise suppression is improved in [25] and [26], the increase of ESO order makes their parameter tuning more complicated. The ESO based on Fal function filter was studied in [27]. It can effectively suppress the measurement noise without increasing the observer order, thus avoiding the difficulty of parameter tuning. In [28], the composite structure of Kalman filter and ESO was introduced to deal with the balance between disturbance rejection of system and noise suppression. The actual measurement signal in the ESO was replaced with the estimation value in Kalman filter, and the lumped disturbance in the ESO was applied to the Kalman filter to improve estimation accuracy. The series structure of filter and observer was used to deal with the contradiction between disturbance rejection performance and noise suppression in [27] and [28]. However, the filter parameters have a certain influence on the control performance because of the lack of accurate noise statistics. The cascaded ESO was considered in [29] and [30] to suppress the high-frequency measurement noise. The cascaded structure also increases the difficulty of parameter tuning because of multiple observers. Considering the measurement noise of speed loop in this article, the adaptive extended state observer (AESO) is proposed to balance the disturbance rejection performance and noise suppression. And the adaptive integral ESO (AIESO) is proposed to improve the tracking accuracy when subject to time-varying disturbance.

Besides, due to the strong dependence of the FCS-MPC on its own system model and the possibility of system parameters variation during operation, the predicted performance is susceptible to parameter uncertainties. For the parameter mismatch problems, the incremental prediction model is considered to eliminate the influence of flux mismatch on system performance and the inductance extraction algorithm is proposed to correct the inductance value in [31]. In [32], an incremental predictive current control method and an online parameter identification algorithm based on model reference adaptive system (MRAS) are proposed to eliminate the influence caused by parameter mismatch. In [33], a robust predictive current control algorithm is proposed to deal with the parameter mismatch problems by applying weight factors. The proposed robust exploration based on FCS-MPCC strategy is studied in [34] to improve the robustness. The parameter mismatch problems can also be solved by using observer or applying model-free predictive current control method [35], [36]. In this article, considering that the parameter mismatch will cause the sector misjudgment, the inductance parameter estimation method and the disturbance compensation mechanism are introduced into the improved multistep FCS-MPCC based on sector to improve the parameter robustness.

Based on the analysis of the above literature, in order to further reduce the calculation burden in [19], the cost function is first modified to reduce the calculation times of predicted values. Second, in order to avoid traversing all the voltage vectors, the sector method is considered to be applied to multistep model predictive current control. Different sector division methods are combined to narrow the control set, which will further reduce the amount of computation. Meanwhile, it is a fact that the high gain ESO will amplify noise. There is poor convergence for low gain ESO. Motivated by the challenge, the AESO is proposed to balance disturbance rejection performance and noise suppression in this article. When the system is disturbed, the real-time gain of the AESO will increase to improve the disturbance rejection performance, and the gain will decrease to enhance noise suppression performance in steady state. However, when the system is disturbed by time-varying disturbance, the steady-state tracking accuracy will become poor because of the small adaptive gain in steady state. Because of this, the AIESO is proposed to improve the tracking accuracy, which not only retains the advantages of AESO but also improves the steady-state tracking accuracy compared with AESO. Considering that the system control performance will deteriorate due to parameter mismatches, the inductance parameter estimation method is proposed to update the initial inductance of the observer and then combine the observer to suppress parameter mismatches. Specifically, the main contributions of this article can be summarized as follows.

1) First, in order to further reduce the calculation amount of multistep FCS-MPCC for current loop used in [19], modifying the cost function to decrease the calculation times of predicted values, and combining the different sector division method to multistep FCS-MPCC. The calculation burden is reduced compared with the original algorithm in [19], but the control performance of the proposed algorithm is consistent with that of the original algorithm.
2) Second, considering the fact that high gain ESO will amplify measurement noise and low gain ESO has poor convergence, AESO is proposed to balance the disturbance rejection performance and noise suppression. However, disturbed by time-varying disturbance, the adaptive gain in steady state will become small, which will lead to poor steady-state tracking accuracy.
3) Third, in order to improve the poor steady-state tracking accuracy caused by time-varying disturbance, the integral

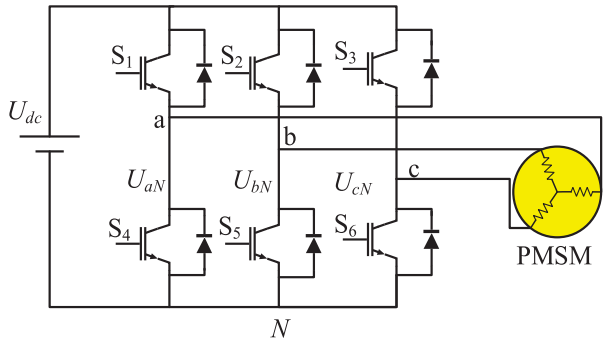

Fig. 1. Inverter-based PMSM drives.

term is combined into the AESO, AIESO is proposed, which not only balances disturbance rejection performance and noise suppression but also improves steady-state tracking accuracy.

4) At last, in order to avoid the sector misjudgment caused by parameter mismatches, the inductance parameter estimation method is proposed and combines disturbance compensation mechanism to improve the robustness of the system to motor parameters.

The rest of this article is organized as follows. In Section II, the mathematical model of PMSM system is introduced. In Section III, the traditional single-step FCS-MPC, multistep FCS-MPC, and the proposed algorithm are described. In Section IV, the MATLAB/Simulink simulation results of the proposed algorithm are shown. The experimental setup and results are shown in Section V. Finally, Section VI concludes this article.

II. Mathematical Model of Permanent Magnet Synchronous Motor System

The mathematical model of PMSM can be described as follows [1]:

$$J\frac{d\omega_m}{dt} = T_e - T_L - B\omega_m \tag{1}$$

$$L_d\frac{di_d}{dt} = u_d - R_s i_d + \omega_{re} L_q i_q \tag{2}$$

$$L_q\frac{di_q}{dt} = u_q - R_s i_q - \omega_{re}\psi_f - \omega_{re} L_d i_d \tag{3}$$

where u_d and i_d represent voltage and current in the d-axis, respectively. u_q and i_q represent voltage and current in the q-axis, respectively. L_d, L_q represent the stator inductance in the $d-q$ axis, $L_d = L_q = L_s$. $R_s, \omega_{re}, \psi_f, \omega_m$ represent the stator resistance, electrical angular velocity of the rotor, flux linkage, mechanical angular velocity of rotor, respectively. J represents the moment of inertia, B represents viscous friction coefficient, and T_e and T_L represent the electromagnetic torque and load torque, respectively.

As shown in Fig. 1, the two-level voltage source inverter is used. U_{aN}, U_{bN}, U_{cN} represent the output voltage of the three bridge arms of the inverter, respectively. U_{dc} represents the dc bus voltage. $S_1 - S_6$ represent the switching state.

III. Adaptive Integral Extended State Observer-Based Improved Multistep FCS-MPCC for PMSM

The control system of PMSM consists of two main parts: 1) current loop controller and 2) speed loop controller. In field oriented control (FOC) strategy, both of these controllers use PI controller, which require parameter tuning and modulation. In this article, the FCS-MPC control method is studied, and the cost function is used as the current loop controller, which does not require complex pulsewidth modulation and parameter tuning, bringing faster dynamic performance. In order to have less computational burden compared with [19], an improved multistep FCS-MPCC based on sector is proposed in the current loop. And the speed controller based on AIESO is designed in the speed loop. On the one hand, the computation burden is decreased compared with [19], but keeps same control performance. On the other hand, the contradiction between disturbance rejection and noise suppression is well balanced, and the steady-state tracking accuracy is improved subject to time-varying disturbance. Finally, in order to avoid the sector misjudgment caused by parameter mismatch, the inductance parameter estimation method is proposed and combines disturbance compensation mechanism to improve the robustness of the system to motor parameters. The control strategy adopted by the whole control system in this article is shown in Fig. 2.

A. Current Loop Design

1) Single-Step FCS-MPCC: Compared with FOC strategy, FCS-MPCC can quickly track current commands and does not require parameter tuning in the current loop, which can make the system obtain good dynamic response characteristics. The discrete form of current prediction model can be obtained from (2) to (3)

$$i(k+1) = Ai(k) + Bu(k) + C \tag{4}$$

where

$$i(k) = \begin{bmatrix} i_d(k) & i_q(k) \end{bmatrix}^T, u(k) = \begin{bmatrix} u_d(k) & u_q(k) \end{bmatrix}^T,$$

$$A = \begin{bmatrix} 1 - \frac{R_s T_s}{L_d} & \frac{L_q T_s}{L_d}\omega_{re}(k) \\ -\frac{L_d T_s}{L_q}\omega_{re}(k) & 1 - \frac{R_s T_s}{L_q} \end{bmatrix}, B = \begin{bmatrix} \frac{T_s}{L_d} \\ \frac{T_s}{L_q} \end{bmatrix},$$

$$C = \begin{bmatrix} 0 \\ -\frac{\psi_f T_s}{L_q}\omega_{re}(k) \end{bmatrix}, T_s$$

is the sample time.

Because there exists computation delay in the actual system, the present optimal voltage vector will be applied to the inverter in the next control period. For this reason, it is necessary to make one-step delay compensation for the system. Equation (6) could be used for one-step compensation, then the predicted current value and cost function value can be obtained by using different voltage vector from the finite voltage vector control set (u_i) into the following (6):

$$i^{\text{pre}}(k+2) = Ai(k+1) + Bu_i + C. \tag{5}$$

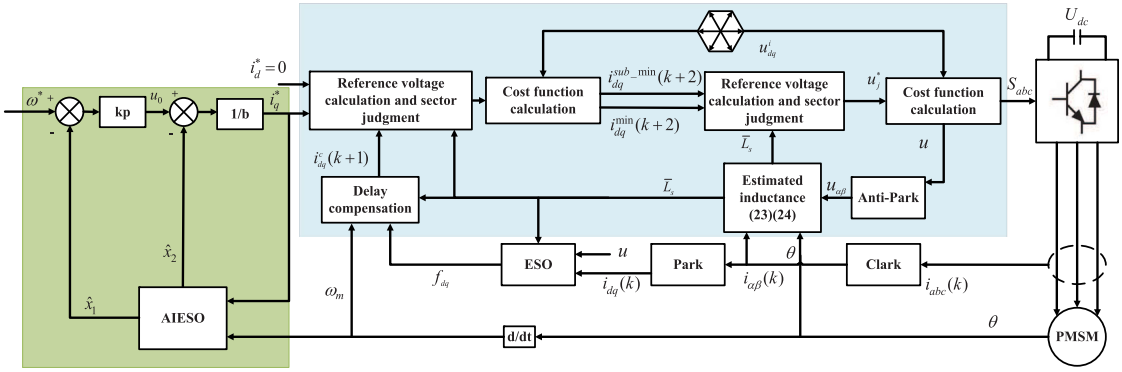

Fig. 2. Proposed control strategy.

In order to better evaluate tracking performance, the cost function form is as follows:

$$g_i = \left\| i_{dq}^* - i_{dq}^{\text{pre}}(k+2) \right\| \tag{6}$$

where $i_{dq}^* = [i_d^* \quad i_q^* \ ]^T$ represent the reference value component of stator current in the $d-q$ axis; $i_{dq}^{\text{pre}}(k+2) = [i_d^{\text{pre}}(k+2) \quad i_d^{\text{pre}}(k+2) \ ]^T$ represent the predicted stator current in $d-q$ axis at $(k+2)T_s$, respectively.

Remark 1: As a two-level inverter is adopted in this article, the number of elements in the voltage vector control set is finite, which will result in unsatisfactory steady-state performance. For this reason, the multistep FCS-MPCC is proposed to improve the system steady-state performance.

2) Multistep FCS-MPCC: Compared with single-step FCS-MPCC, multistep FCS-MPCC can improve the steady-state performance of the system to some extent. Assuming that the speed of PMSM does not change significantly in the prediction horizon and delay compensation is considered, the prediction model of multistep FCS-MPCC is shown as follows:

$$i^{\text{pre}}(k+N) = Ai^{\text{pre}}(k+N-1) + Bu_i + C \tag{7}$$

where N is the prediction horizon, and $N > 2$.

The corresponding cost function form is

$$g = \sum_{n=2}^{N} \left\| i_{dq}^* - i_{dq}^{\text{pre}}(k+n) \right\|. \tag{8}$$

However, with the increase of the prediction horizon, the voltage vector combination will increase exponentially, which makes it difficult to apply the multistep FCS-MPCC strategy to practical applications. An improved multistep FCS-MPCC based on sector is proposed to reduce the computational burden in this article.

3) Improved Multistep FCS-MPCC With Low Parameter Sensitivity Based on Sector: In traditional FCS-MPCC, the cost function based on current error is viewed as the current loop controller. However, eight times of predicted value calculation should be carried out according to the prediction model during the control process. In order to reduce the amount of calculation, the cost function based on voltage error is taken. The new cost function is

$$g_i = \left\| u_{dq}^* - u_{dq}^i \right\|. \tag{9}$$

The voltage vectors corresponding to subminimum value and minimum value of cost function values are represented as $u_{\text{sub\_min}}$ and $u_{\min}$, respectively

$$\begin{cases} u_{\text{sub\_min}} = \arg\ \text{sub\_min}\{g_i\} \\ u_{\min} = \arg\ \min\{g_i\} \\ u_{\text{sub\_min}}, u_{\min} \in \{u_i, i = 0,1,2,3,4,5,6,7\}. \end{cases} \tag{10}$$

In order to reduce the impact of delay on control performance, one-step current prediction is adopted to realize delay compensation

$$i_{dq}^c(k+1) = Ai_{dq}(k) + Bu_{dq}^{\text{pre}} + C. \tag{11}$$

The predicted reference voltage equation after delay compensation is

$$u_{dq}^* = \bar{A}i_{dq}^c + \bar{B}i_{dq}^* + \bar{C} \tag{12}$$

where

$$i_{dq}^* = \begin{bmatrix} i_d^* & i_q^* \end{bmatrix}^T,\ i_{dq}^c = \begin{bmatrix} i_d^c & i_q^c \end{bmatrix}^T$$

$$u_{dq}^* = \begin{bmatrix} u_d^* & u_q^* \end{bmatrix}^T,\ \bar{A} = \begin{bmatrix} R_s - \frac{L_s}{T_s} & -L_s\omega_{re} \\ L_s\omega_{re} & R_s - \frac{L_s}{T_s} \end{bmatrix}$$

$$\bar{B} = \begin{bmatrix} \frac{L_s}{T_s} & \frac{L_s}{T_s} \end{bmatrix}^T,\ \bar{C} = \begin{bmatrix} 0 & \omega_{re}\psi_f \end{bmatrix}^T.$$

The predicted reference voltage in the $\alpha-\beta$ coordinate is

$$\begin{bmatrix} u_\alpha^* \\ u_\beta^* \end{bmatrix} = \begin{bmatrix} \cos\theta & -\sin\theta \\ \sin\theta & \cos\theta \end{bmatrix} \begin{bmatrix} u_d^* \\ u_q^* \end{bmatrix}. \tag{13}$$

Calculate the sector position of the predicted reference voltage

$$\begin{cases} H_0 = u_\alpha^* \\ H_1 = -\frac{1}{2}u_\alpha^* + \frac{\sqrt{3}}{2}u_\beta^* \\ H_2 = -\frac{1}{2}u_\alpha^* - \frac{\sqrt{3}}{2}u_\beta^*. \end{cases} \tag{14}$$

The serial number of the sector is

$$H = 4\text{sgn}(H_2) + 2\text{sgn}(H_1) + \text{sgn}(H_0) \tag{15}$$

TABLE I
RELATIONSHIP BETWEEN H AND SECTORS

H	1	2	3	4	5	6
Sector	I	III	II	IV	V	VI

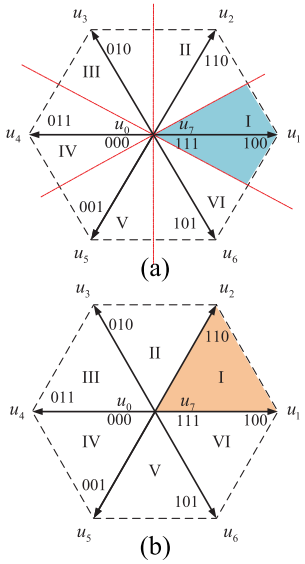

Fig. 3. Sector division method. (a) Two vector. (b) Three vector.

where $\mathrm{sgn}(x) = \begin{cases} 1 & x \geq 0 \\ 0 & x < 0 \end{cases}$.

As is shown in Table I, the value H is used to determine the sector position of the predicted reference voltage.

The sector division method in Fig. 3(a) can effectively ensure that there is only one nonzero vector and two zero vectors in each sector. In single-step FCS-MPCC, the cost function value corresponding to the nonzero vector and the zero vector can be compared to output the optimal voltage vector. This sector division method can effectively reduce the times of predicted values and cost function optimization. However, the multistep FCS-MPCC algorithm proposed in [19] involves optimal voltage vector and suboptimal voltage vector, the selection process of suboptimal voltage vector will become complicated if the sector division method in Fig. 3(a) is used to select the suboptimal voltage vector. Therefore, the division method in Fig. 3(b) is considered to simplify the selection process of suboptimal voltage. At the same time, considering the sector division method in Fig. 3(a) can simplify the selection process of the optimal voltage vector, two different sector division methods can be combined with the multistep FCS-MPCC to improve the steady-state performance of the system without significantly increasing the calculation burden.

Similar to the process to locate the voltage vector in Fig. 3(a), it is easy to obtain the relationship between the serial numbers G and sectors in Fig. 3(b) by interchanging u_α^* and u_β^*, as shown in Table II.

TABLE II
RELATIONSHIP BETWEEN G AND SECTORS

G	1	2	3	4	5	6
Sector	III	I	V	IV	VI	II

TABLE III
COMPARISON OF PREDICTION TIMES

multi-step predictive control	times
traditional multi-step predictive control	72
multi-step predictive control [17]	16
multi-step predictive control [19]	24
multi-step predictive control in this article	10

With the predicted step size $N = 3$, The predicted current value after delay compensation is

$$i_{dq}^p(k+2) = Ai_{dq}^c(k+1) + Bu_{dq}^i + C. \tag{16}$$

In the second step of prediction, the predicted reference voltage can be expressed as

$$u_j^* = \bar{A}i_{dq}^j(k+2) + \bar{B}i_{dq}^* + \bar{C} \tag{17}$$

where $j \in \{\min, \text{sub\_min}\}$, $i_{dq}^j(k+2) \in i_{dq}^p(k+2)$.

At this point, the cost function is

$$g = \begin{bmatrix} A \\ B \end{bmatrix} = \begin{bmatrix} \left\| u_{\min}^* - u_{dq}^i \right\| & \left\| u_{\min}^* \right\| \\ \left\| u_{\text{sub\_min}}^* - u_{dq}^i \right\| & \left\| u_{\text{sub\_min}}^* \right\| \end{bmatrix}. \tag{18}$$

Then the voltage vector ultimately acting on the inverter is

$$u_{\text{out}} = \begin{cases} u_{\min} & \text{if} \quad \min(g) \in A \\ u_{\text{sub\_min}} & \text{if} \quad \min(g) \in B. \end{cases} \tag{19}$$

In order to verify the effectiveness of the proposed algorithm in the current loop, the prediction times of several multistep predictive control methods are compared for the case $N = 3$, as is shown in Table III. The improved multistep FCS-MPCC based on sector is not only suitable for the case $N = 3$, but also can be extended to a longer prediction horizon.

Depending on the specific form of the ESO, it is easy to see that providing an initial inductance value for the observer design is necessary. If the initial inductance value is not appropriate, the estimation burden of the observer will be increased. Therefore, a rough estimation method of inductance parameter is proposed in this article to provide a relatively accurate initial inductance value to reduce the estimated burden of the observer. The rest of the disturbance is solved by the observer. In addition, because the estimated inductance value is obtained by using the voltage, current, and position information of the system, it is relatively closer to the real value. Considering that the inductance value has a great influence on the system performance. Therefore, it is reasonable to update the estimated inductance value to the prediction model to improve the system performance. In a word, the inductance parameter estimation method in this article can be combined with the observer to update the initial inductance value, which can help to suppress the parameter mismatches with a smaller estimated burden of the observer. When the parameters

do not match, the robustness of the system to the parameters is improved by using the observer with the updated inductance parameter

$$\begin{cases} i_\alpha(k)-i_\alpha(k-1)=\frac{T_s}{\bar{L}_s}[u_\alpha(k-1)-\bar{R}i_\alpha(k-1) \\ \qquad\qquad +\bar{\psi}_f\omega_{re}\sin(\theta(k-1))] \\ i_\beta(k)-i_\beta(k-1)=\frac{T_s}{\bar{L}_s}[u_\beta(k-1)-\bar{R}i_\beta(k-1) \\ \qquad\qquad +\bar{\psi}_f\omega_{re}(k-1)\cos(\theta(k-1))]. \end{cases} \tag{20}$$

According to (20), the following can be obtained:

$$\begin{aligned} &\frac{T_s}{\bar{L}_s}[u_\alpha(k-1)\cos(\theta(k-1))+u_\beta(k-1)\sin(\theta(k-1)) \\ &\quad -\bar{R}(i_\alpha(k-1)\cos(\theta(k-1))+i_\beta(k-1)\sin(\theta(k-1)))] \\ &\quad =(i_\beta(k)-i_\beta(k-1))\sin(\theta(k-1)) \\ &\qquad +(i_\alpha(k)-i_\alpha(k-1))\cos(\theta(k-1)). \end{aligned} \tag{21}$$

Ignoring the resistance voltage drop, (21) can be written as

$$\begin{aligned} &\frac{T_s}{\bar{L}_s}[u_\alpha(k-1)\cos(\theta(k-1))+u_\beta(k-1)\sin(\theta(k-1))] \\ &\quad \approx (i_\beta(k)-i_\beta(k-1))\sin(\theta(k-1)) \\ &\quad +(i_\alpha(k)-i_\alpha(k-1))\cos(\theta(k-1)). \end{aligned} \tag{22}$$

Let $K=\frac{T_s}{\bar{L}_s}$, it can be obtain

$$\begin{aligned} K=&[(i_\alpha(k)-i_\alpha(k-1))\cos(\theta(k-1)) \\ &+(i_\beta(k)-i_\beta(k-1))\sin(\theta(k-1))] \\ &/[u_\alpha(k-1)\cos(\theta(k-1))+u_\beta(k-1)\sin(\theta(k-1))]. \end{aligned} \tag{23}$$

When the sampling period is short, the inductance can be estimated according to K, which can be used to update the initial inductance of observer to deal with parameter mismatches with a smaller estimated burden. And the estimated inductance is also used to update the prediction model to improve the system performance. The above method can be considered to improve the robustness of the system to the inductance parameter L_s

$$\bar{L}_s=\frac{T_s}{K}. \tag{24}$$

The other parameter mismatches will also lead to the selection of the wrong voltage vector. In order to reduce the influence caused by other parameters, the ESO with updated inductance is considered to deal with the parameter mismatches with a smaller estimated burden.

Let $x_{1\,d}=i_d, x_{2\,d}=f_d, \dot{x}_{2\,d}=h_d$, and h_d is bounded, then (2) can be written as

$$\begin{cases} \dot{x}_{1\,d}=\frac{u_d}{\bar{L}_s}+x_{2\,d} \\ \dot{x}_{2\,d}=h_d. \end{cases} \tag{25}$$

According to (25), the d-axis observer is designed as follows:

$$\begin{cases} \dot{z}_{1\,d}=\frac{u_d}{\bar{L}_s}+z_{2\,d}+\beta_{1\,d}(x_{1\,d}-z_{1\,d}) \\ \dot{z}_{2\,d}=\beta_{2\,d}(x_{1\,d}-z_{1\,d}). \end{cases} \tag{26}$$

The q-axis observer design is similar to the d-axis observer

$$\begin{cases} \dot{z}_{1q}=\frac{u_q}{\bar{L}_s}+z_{2q}+\beta_{1q}(x_{1q}-z_{1q}) \\ \dot{z}_{2q}=\beta_{2q}(x_{1q}-z_{1q}) \end{cases} \tag{27}$$

where $\beta_{1\,d}, \beta_{1q,\beta_{2\,d},\beta_{2\,d}}$ represent the observer gain, satisfying the condition that $\beta_{1\,d}=\beta_{1q}=2\omega_d$ and $\beta_{2\,d}=\beta_{2q}=\omega_d^2$. f_d, f_q represent lumped disturbance. By using the observer to compensate the disturbance caused by parameter mismatch, the robustness of the system to stator resistance R_s and flux linkage ψ_f can be improved to some extent.

B. Speed Loop Design

1) ESO-Based Improved Multistep FCS-MPCC: Considering that the speed loop is susceptible to model parameter uncertainty and external disturbance, ESO is considered to be applied to speed loop to improve disturbance rejection performance for PMSM.

Let $x_1=\omega_m, x_2=-\frac{B\omega_m}{J}-\frac{T_L}{J}+\frac{3p\psi_f}{2J}i_q-bi_q{}^*$, then (1) is arranged into the form of state space

$$\begin{cases} \dot{x}_1=bi_q^*+x_2 \\ \dot{x}_2=h \end{cases} \tag{28}$$

where x_2 represents lumped disturbance, h represents the derivative of lumped disturbance, and p represents the pole pairs.

According to (28), the observer is designed as follows:

$$\begin{cases} \dot{\hat{x}}_1=bi_q^*+\hat{x}_2-\beta_1(\hat{x}_1-x_1) \\ \dot{\hat{x}}_2=-\beta_2(\hat{x}_1-x_1) \end{cases} \tag{29}$$

where $\hat{x}_1$ represents the estimated value of state variable x_1, $\hat{x}_2$ represents the estimated value of lumped disturbance x_2, and β_1, β_2 represent the observer gain.

The observer error equation can be obtained by subtracting (29) from (28)

$$\begin{bmatrix} \dot{e}_1 \\ \dot{e}_2 \end{bmatrix}=\begin{bmatrix} -\beta_1 & 1 \\ -\beta_2 & 0 \end{bmatrix}\begin{bmatrix} e_1 \\ e_2 \end{bmatrix}+\begin{bmatrix} 0 \\ 1 \end{bmatrix}h \tag{30}$$

where $e_1=x_1-\hat{x}_1, e_2=x_2-\hat{x}_2$.

The characteristic equation of the error equation is

$$P(s)=s^2+\beta_1 s+\beta_2. \tag{31}$$

Assume that the expected poles of the system $\lambda_1=\lambda_2=-\omega(\omega>0)$ are true, then

$$P(s)=s^2+\beta_1 s+\beta_2=(s+\omega)^2=s^2+2\omega s+\omega^2 \tag{32}$$

so $\beta_1=2\omega, \beta_2=\omega^2$ can be obtained.

As long as the parameter ω are properly selected, the estimated speed $\hat{x}_1$ and the estimated lumped disturbance $\hat{x}_2$ can be obtained through the ESO. However, the fixed observer gain does not improve both disturbance rejection and noise suppression. The analysis of disturbance rejection and noise suppression about ESO is shown as follows.

Let $u=i_q^*$, the Laplace transform of (29) can be obtained

$$\begin{cases} s\hat{X}_1=bU+\hat{X}_2-\beta_1(\hat{X}_1-X_1) \\ s\hat{X}_2=-\beta_2(\hat{X}_1-X_1). \end{cases} \tag{33}$$

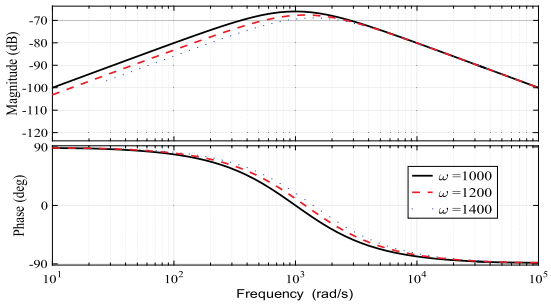

Fig. 4. Amplitude-frequency response curves of (35) under different gains.

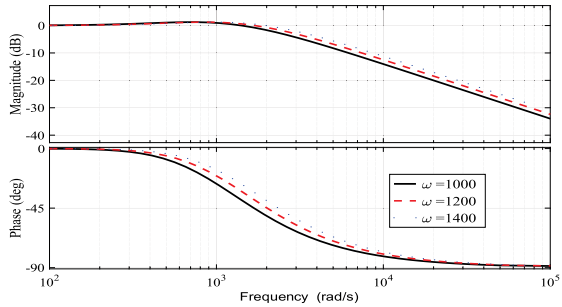

Fig. 5. Amplitude-frequency response curves of (36) under different gains.

Rearranging (33), it can be obtained

$$\begin{cases} \hat{X}_1 = \frac{\beta_1 s+\beta_2}{s^2+\beta_1 s+\beta_2} X_1 + \frac{bs}{s^2+\beta_1 s+\beta_2} U \\ \hat{X}_2 = \frac{\beta_2 s}{s^2+\beta_1 s+\beta_2} X_1 - \frac{b\beta_2}{s^2+\beta_1 s+\beta_2} U. \end{cases} \tag{34}$$

In order to more accurately analyze the impact of observer gain on disturbance rejection and noise suppression performance, the analysis is carried out from four cases.

Case I: Consider the influence of disturbance on estimated value $\hat{X}_1$.

According to (34), the transfer function between disturbance F and the estimated value $\hat{X}_1$ can be obtained as follows:

$$\frac{\hat{X}_1}{F} = \frac{bs}{s^2+\beta_1 s+\beta_2}. \tag{35}$$

Case II: Consider the influence of noise on estimated value $\hat{X}_1$.

According to (34), the transfer function between noise V and the estimated value $\hat{X}_1$ can be obtained as

$$\frac{\hat{X}_1}{V} = \frac{\beta_1 s+\beta_2}{s^2+\beta_1 s+\beta_2}. \tag{36}$$

Case III: Consider the influence of disturbance on estimated value $\hat{X}_2$.

According to (34), the transfer function between disturbance F and the estimated value $\hat{X}_2$ can be obtained as

$$\frac{\hat{X}_2}{F} = -\frac{b\beta_2}{s^2+\beta_1 s+\beta_2}. \tag{37}$$

Case IV: Consider the influence of noise on estimated value $\hat{X}_2$.

According to (34), the transfer function between noise V and the estimated value $\hat{X}_2$ can be obtained as

$$\frac{\hat{X}_2}{V} = \frac{\beta_2 s}{s^2+\beta_1 s+\beta_2}. \tag{38}$$

The corresponding Bode diagrams for the four cases are shown in Figs. 4–7, respectively. As shown in Fig. 4, it is obvious that there is strong disturbance rejection on low-frequency disturbance, when selecting the higher observer gain. However, there is poor noise suppression with high gain in Fig. 5. In Fig. 6, the low-frequency disturbance rejection performance is almost the same when different gains are selected. Similar to

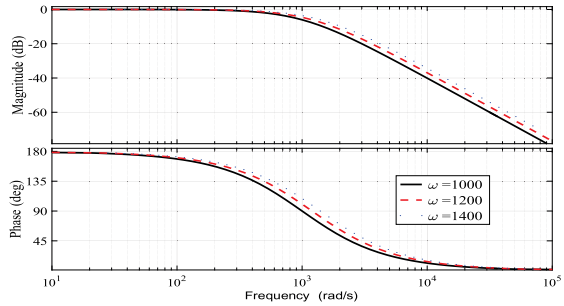

Fig. 6. Amplitude-frequency response curves of (37) under different gains.

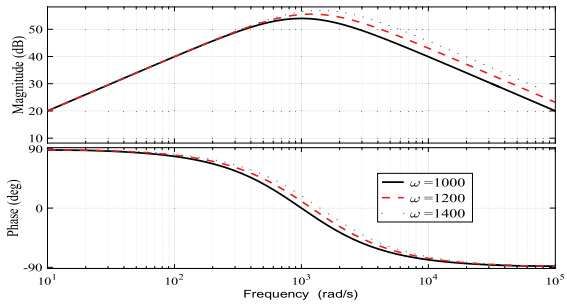

Fig. 7. Amplitude-frequency response curves of (38) under different gains.

the conclusion in Fig. 5, the noise suppression performance is gradually weakened as the observer gain increases in Fig. 7. In a word, the conclusion will be drawn that high gain can improve the disturbance rejection but amplify the measurement noise.

Because of strong disturbance rejection of high gain, the high gain is often considered in theory. However, the measured speed is subject to measurement noise in practice, the measurement noise will be amplified by high gain. In order to deal with the contradiction, AESO is proposed in the following to balance between disturbance rejection and noise suppression.

2) AESO-Based Improved Multistep FCS-MPCC: The form of AESO is shown as follows:

$$\begin{cases} e_1 = x_1 - z_1 \\ \dot{z}_1 = z_2 + \beta_1(\omega)e_1 + bi_q^* \\ \dot{z}_2 = \beta_2(\omega^2)e_1 \end{cases} \tag{39}$$

where $\omega = \omega_{\min} + (\omega_{\max} - \omega_{\min}) * \frac{2}{\pi} * \operatorname{atan}(k * |e_1|)^m$.

The design process of the corresponding controller is as follows.

Let $u_0 = bi_q^* + x_2$, the lumped disturbance estimation value z_2 obtained by the observer is used to replace x_2, then the reference current value of the current loop in the q-axis can be obtained after disturbance compensation

$$i_q^* = \frac{u_0 - z_2}{b}. \tag{40}$$

The linear state error feedback control law is adopted for u_0, so the control law based on disturbance compensation can be obtained

$$i_q^* = \frac{k_p(\omega^* - z_1) - z_2}{b} \tag{41}$$

where k_p is the proportional gain.

Assumption 1: Assume the lumped disturbance x_2 and the derivative of lumped disturbance h are bounded.

Theorem 1: If (28) satisfies Assumption 1, the estimation error of AESO is bounded.

Proof: Define the estimated error variable: $e_1 = x_1 - z_1$, $e_2 = x_2 - z_2$, then the estimation error equation is

$$\dot{e} = A_e e + B_e h \tag{42}$$

where $e = \begin{bmatrix} e_1 & e_2 \end{bmatrix}^T$, $A_e = \begin{bmatrix} -\beta_1(\omega) & 1 \\ -\beta_2(\omega^2) & 0 \end{bmatrix}$, $B_e = \begin{bmatrix} 0 & 1 \end{bmatrix}^T$.

To facilitate parameter adjustment, let $\beta_1(\omega) = \beta_1\omega, \beta_2(\omega) = \beta_2\omega^2$, then the estimation error equation can be expressed as

$$\begin{bmatrix} \dot{e}_1 \\ \dot{e}_2 \end{bmatrix} = \begin{bmatrix} -\beta_1\omega & 1 \\ -\beta_2\omega^2 & 0 \end{bmatrix} \begin{bmatrix} e_1 \\ e_2 \end{bmatrix} + \begin{bmatrix} 0 \\ 1 \end{bmatrix} h. \tag{43}$$

Let $\varepsilon_i = \frac{e_i}{\omega^{i-1}}, i = 1, 2$, then

$$\dot{\varepsilon} = \omega A_\varepsilon \varepsilon + B_\varepsilon \frac{h}{\omega} \tag{44}$$

where $\varepsilon = \begin{bmatrix} \varepsilon_1 & \varepsilon_2 \end{bmatrix}^T$, $A_\varepsilon = \begin{bmatrix} -\beta_1 & 1 \\ -\beta_2 & 0 \end{bmatrix}$, $B_\varepsilon = \begin{bmatrix} 0 & 1 \end{bmatrix}^T$.

The solution of the estimation error equation (44) can be expressed as

$$\varepsilon(t) = e^{\omega A_\varepsilon t}\varepsilon(0) + \int_0^t e^{\omega A_\varepsilon (t-\tau)} B_\varepsilon \frac{h}{\omega} d\tau \tag{45}$$

where $\varepsilon(0) = [\varepsilon_1(0) \quad \varepsilon_2\ (0)]^T = [e_1(0) \quad \frac{e_2(0)}{\omega}\ ]^T$.

Since the derivative of lumped disturbance h is assumed to be bounded, there exists a positive real N number such that $|h| \le N$.

Let $\varphi(t) = \int_0^t e^{\omega A_\varepsilon (t-\tau)} B_\varepsilon \frac{h}{\omega} d\tau$, then

$$\begin{aligned} |\varphi_i(t)| &\le \frac{N}{\omega} \int_0^t e^{\omega A_\varepsilon (t-\tau)} B_\varepsilon d\tau \\ &\le \frac{N}{\omega^2}\left(\left|A_\varepsilon^{-1} B_\varepsilon\right| + \left|A_\varepsilon^{-1} e^{\omega A_\varepsilon t} B_\varepsilon\right|\right). \end{aligned} \tag{46}$$

Selecting the appropriate β_1, β_2 such that the matrix A_ε is the Hurwitz matrix, thus there is a time constant $T(T > 0)$. When $t > T$ is true, then

$$\left|\left[e^{\omega A_\varepsilon t}\right]_{ij}\right| \le \frac{1}{\omega^2} \tag{47}$$

$$\left|\left[e^{\omega A_\varepsilon t} B_\varepsilon\right]_i\right| \le \frac{1}{\omega^2} \tag{48}$$

where $i, j = 1, 2$.

The inverse matrix A_ε^{-1} can be easily derived from the matrix A_ε

$A_\varepsilon^{-1} = \begin{bmatrix} 0 & -\frac{1}{\beta_2} \\ 1 & -\frac{\beta_1}{\beta_2} \end{bmatrix}$ thus

$$\left|\left[A_\varepsilon^{-1} B_\varepsilon\right]_i\right| = \left|\begin{bmatrix} -\frac{1}{\beta_2} \\ -\frac{\beta_1}{\beta_2} \end{bmatrix}_i\right| = \left.\begin{matrix} \frac{1}{\beta_2} \\ \frac{\beta_1}{\beta_2} \end{matrix}\right|_{i=2}^{i=1} \le \gamma \tag{49}$$

where $\gamma = \max\{\frac{1}{\beta_2}, \frac{\beta_1}{\beta_2}\}$.

According to (48) and the inverse matrix A_ε^{-1}, the following equation can be obtained for the case $(t > T)$:

$$\left|\left[A_\varepsilon^{-1} e^{\omega A_\varepsilon t} B_\varepsilon\right]_i\right| \le \left.\begin{matrix} \frac{1}{\omega^2\beta_2} \\ \frac{1}{\omega^2}\left(1 + \frac{\beta_1}{\beta_2}\right) \end{matrix}\right|_{i=2}^{i=1} \le \frac{\eta}{\omega^2} \tag{50}$$

where $\eta = \max\{\frac{1}{\beta_2}, (1 + \frac{\beta_1}{\beta_2})\}$.

It is easy to get the following result from (49) and (50):

$$|\varphi_i(t)| \le \frac{N}{\omega^2}\left(\gamma + \frac{\eta}{\omega^2}\right) = \frac{N\gamma}{\omega^2} + \frac{N\eta}{\omega^4}. \tag{51}$$

From (47), we can obtain

$$\left|\left[e^{\omega A_\varepsilon t}\varepsilon(0)\right]_i\right| \le \frac{|\varepsilon_1(0)| + |\varepsilon_2(0)|}{\omega^2}. \tag{52}$$

Thus,

$$\begin{aligned} |\varepsilon_i(t)| = \left|\left[e^{\omega A_\varepsilon t}\varepsilon(0)\right]_i\right| + |\varphi_i(t)| &\le \frac{|\varepsilon_1(0)| + |\varepsilon_2(0)|}{\omega^2} \\ &+ \frac{N\gamma}{\omega^2} + \frac{N\eta}{\omega^4}. \end{aligned} \tag{53}$$

Equation (53) can also be expressed as

$$|e_i(t)| \le \frac{|e_1(0)| + |e_2(0)|}{\omega^2} + \frac{N\gamma}{\omega^{3-i}} + \frac{N\eta}{\omega^{5-i}}. \tag{54}$$

Because the condition $\omega_{\min} \le \omega \le \omega_{\max}$ is satisfied, the upper bound of estimation error can be expressed as

$$|e_i(t)| \le \frac{|e_1(0)| + |e_2(0)|}{\omega_{\min}^2} + \frac{N\gamma}{\omega_{\min}^{3-i}} + \frac{N\eta}{\omega_{\min}^{5-i}} \quad \forall t > T. \tag{55}$$

■

Remark 2: From (55), it is easy to know that the estimation error of AESO is bounded, and its upper bound is related to the initial estimation error, the upper bound of the derivative of the lumped disturbance, and the observer gain. With the decrease of observer gain, the estimation error of observer will increase gradually.

Next, the relationship between the estimation error and gain of AESO will be analyzed when disturbed by different types of disturbances.

The Laplace transform of the (43) can be expressed as

$$\begin{cases} sE_1 = -\beta_1\omega E_1 + E_2 \\ sE_2 = -\beta_2\omega^2 E_1 + sF. \end{cases} \tag{56}$$

From (56), the transfer function from the lumped disturbance to estimation error e_1 can be obtained

$$\frac{E_1}{F} = \frac{s}{s^2 + \beta_1\omega s + \beta_2\omega^2}. \tag{57}$$

When the lumped disturbance is constant disturbance and time-varying disturbance, respectively, the corresponding Laplace transform is $F = \frac{1}{s}, F = \frac{1}{s^2}$, the steady-state estimation error can be obtained according to the final-value theorem

$$e_1(\infty) = \begin{cases} 0 & \left(F = \frac{1}{s}\right) \\ \frac{1}{\beta_2\omega^2} & \left(F = \frac{1}{s^2}\right). \end{cases} \tag{58}$$

It can be seen from (58) that when the system is disturbed by time-varying disturbance, the steady-state estimation error of the observer will increase with the decrease of the observer gain.

Theorem 2: Suppose that Assumption 1 is satisfied. The bounded stability of (28) under the control law (41) for any bounded x_2 and h is guaranteed if the observer gain in (39) and controller gain in (41) are chosen such that $\bar{A}_\varepsilon$ is the Hurwitz matrix and $k_p > 0$.

Proof: The control objective of PMSM speed control system is to track the reference speed. Define the tracking error as $\delta = \omega^* - \omega$, then

$$\dot{\delta} = \dot{\omega}^* - \dot{\omega} = -bi_q^* - x_2. \tag{59}$$

According to (28) and (44), it can be obtained

$$\begin{aligned} \dot{\delta} &= \dot{\omega}^* - k_p\delta + \begin{bmatrix} -k_p & -1 \end{bmatrix} e \\ &= \dot{\omega}^* - k_p\delta + \begin{bmatrix} -k_p & -\omega \end{bmatrix} \varepsilon. \end{aligned} \tag{60}$$

The reference speed value given in this article is constant, so

$$\dot{\delta} = -k_p\delta + \begin{bmatrix} -k_p & -\omega \end{bmatrix} \varepsilon. \tag{61}$$

The error equation (44) is rewritten as

$$\dot{\varepsilon} = \omega A_\varepsilon \varepsilon + B_\varepsilon \frac{h}{\omega} = \bar{A}_\varepsilon \varepsilon + \bar{B}_\varepsilon h. \tag{62}$$

In order to ensure the stability of the closed-loop system, the tracking error equation and the estimation error equation can be obtained as

$$\begin{bmatrix} \dot{\delta} \\ \dot{\varepsilon} \end{bmatrix} = \begin{bmatrix} -k_p & \begin{bmatrix} -k_p & -\omega \end{bmatrix} \\ 0 & \bar{A}_\varepsilon \end{bmatrix} \begin{bmatrix} \delta \\ \varepsilon \end{bmatrix} + \begin{bmatrix} 0 \\ \bar{B}_\varepsilon \end{bmatrix} h. \tag{63}$$

Supposing the derivative of lumped disturbance is bounded, it is easy to get the conclusion that the tracking error and the estimation error are bounded if the matrix $\bar{A}_\varepsilon$ is the Hurwitz matrix and the condition $k_p > 0$ is true. ■

In order to further investigate the performance of AESO proposed in this article, different disturbance types are considered to study the effect of AESO gain on the tracking accuracy. First, the Laplace transform of the (43) and (60) can be obtained

$$\begin{cases} s\Delta = -k_p\Delta - k_pE_1 - E_2 \\ sE_1 = -\beta_1\omega E_1 + E_2 \\ sE_2 = -\beta_2\omega^2 E_1 + sF. \end{cases} \tag{64}$$

From the above equation (64), the transfer function from the lumped disturbance to tracking error can be obtained

$$\frac{\Delta}{F} = \frac{-s(s + \beta_1\omega + k_p)}{(s + k_p)(s^2 + \beta_1\omega s + \beta_2\omega^2)}. \tag{65}$$

When the disturbance form is constant disturbance, that is, $F = \frac{1}{s}$, the steady-state tracking error can be obtained according to the final-value theorem

$$\begin{aligned} \delta(\infty) &= \lim_{s\to 0} s\Delta F \\ &= \lim_{s\to 0} \frac{s^2(s + \beta_1\omega + k_p)}{(s + k_p)(s^2 + \beta_1\omega s + \beta_2\omega^2)} \cdot \frac{1}{s} = 0. \end{aligned} \tag{66}$$

If the disturbance form is time-varying disturbance, that is, $F = \frac{1}{s^2}$, the steady-state tracking error can be obtained according to the final-value theorem

$$\begin{aligned} \delta(\infty) &= \lim_{s\to 0} s\Delta F \\ &= \lim_{s\to 0} \frac{s^2(s + \beta_1\omega + k_p)}{(s + k_p)(s^2 + \beta_1\omega s + \beta_2\omega^2)} \cdot \frac{1}{s^2} \\ &= \frac{\beta_1\omega + k_p}{k_p\beta_2\omega^2} \\ &= \frac{\beta_1\omega + k_p}{k_p} e_1(\infty). \end{aligned} \tag{67}$$

When the system disturbed by time-varying disturbance returns to steady state, the adaptive gain of AESO will decrease to improve noise suppression. However, it is obvious that this will lead to a relatively large estimation error according to (58). According to (67), it can be known that the steady-state tracking accuracy will deteriorate due to the large estimation error. In order to improve the steady-state tracking accuracy caused by time-varying disturbance, AIESO is proposed to deal with this problem.

3) AIESO-Based Improved Multistep FCS-MPCC: Different from AESO, the integral term is consider in AIESO, which can not only deal with noise but also improve steady-state tracking accuracy. The specific form of AIESO can be described as

$$\begin{cases} \bar{e}_1 = x_1 - \bar{z}_1 \\ \dot{\bar{z}}_1 = \bar{z}_2 + \bar{\beta}_1(\omega)\bar{e}_1 + bi_q^* \\ \dot{\bar{z}}_2 = \bar{\beta}_2(\omega^2)\bar{e}_1 + \bar{\beta}_3(\omega^3)\int \bar{e}_1 \end{cases} \tag{68}$$

where $\omega = \omega_{\min} + (\omega_{\max} - \omega_{\min}) * \frac{2}{\pi} * \operatorname{atan}(k * |\bar{e}_1|)^m$.

In order to track the reference speed, the control law is designed as follows:

$$i_q^* = \frac{k_{p1}(\omega^* - \bar{z}_1) - \bar{z}_2}{b} \tag{69}$$

where k_{p1} is the proportional gain.

Assumption 2: Assume the second derivatives of lumped disturbances are bounded, that is $|\dot{h}| \le M$.

If Assumption 2 is satisfied, (28) can be arranged in the following form:

$$\begin{cases} \dot{x}_1 = bi_q^* + x_2 \\ \dot{x}_2 = x_3 \\ \dot{x}_3 = \dot{h}. \end{cases} \tag{70}$$

Theorem 3: If (70) satisfies Assumption 2, the estimation error of AIESO is bounded.

Proof: Regard $\bar{z}_3 = \bar{\beta}_3(\omega^3)\int \bar{e}_1$ as a new state variable, define the estimation error variable $\bar{e}_1 = x_1 - \bar{z}_1, \bar{e}_2 = x_2 - \bar{z}_2, \bar{e}_3 = x_3 - \bar{z}_3$, then the estimation error equation is

$$\dot{\bar{e}} = A_{\bar{e}}\bar{e} + B_{\bar{e}}\dot{h} \tag{71}$$

where

$$\bar{e} = \begin{bmatrix}\bar{e}_1 & \bar{e}_2 & \bar{e}_3\end{bmatrix}^T$$

$$A_{\bar{e}} = \begin{bmatrix}-\bar{\beta}_1(\omega) & 1 & 0\\ -\bar{\beta}_2(\omega^2) & 0 & 1\\ -\bar{\beta}_3(\omega^3) & 0 & 0\end{bmatrix}, B_{\bar{e}} = [0 \quad 0 \quad 1]^T.$$

Let $\bar{\beta}_1(\omega) = \bar{\beta}_1\omega, \bar{\beta}_2(\omega) = \bar{\beta}_2\omega^2, \bar{\beta}_3(\omega) = \bar{\beta}_3\omega^3$, thus the estimation error equation is written as

$$\begin{bmatrix}\dot{\bar{e}}_1\\ \dot{\bar{e}}_2\\ \dot{\bar{e}}_3\end{bmatrix} = \begin{bmatrix}-\bar{\beta}_1\omega & 1 & 0\\ -\bar{\beta}_2\omega^2 & 0 & 1\\ -\bar{\beta}_3\omega^3 & 0 & 0\end{bmatrix}\begin{bmatrix}\bar{e}_1\\ \bar{e}_2\\ \bar{e}_3\end{bmatrix} + \begin{bmatrix}0\\ 0\\ 1\end{bmatrix}\dot{h}. \tag{72}$$

Take $\bar{\varepsilon}_i = \frac{\bar{e}_i}{\omega^{i-1}}$, $i = 1, 2, 3$, then

$$\dot{\bar{\varepsilon}} = \omega A_{\bar{\varepsilon}}\varepsilon + B_{\bar{\varepsilon}}\frac{\dot{h}}{\omega^2} \tag{73}$$

where

$$\bar{\varepsilon} = [\bar{\varepsilon}_1 \quad \bar{\varepsilon}_2 \quad \bar{\varepsilon}_3]^T, A_{\bar{\varepsilon}} = \begin{bmatrix}-\bar{\beta}_1 & 1 & 0\\ -\bar{\beta}_2 & 0 & 1\\ -\bar{\beta}_3 & 0 & 0\end{bmatrix}, B_{\bar{\varepsilon}} = [0 \quad 0 \quad 1]^T$$

.

Similar to the previous analysis to prove the convergence of AESO, the estimation error of AIESO is

$$|\bar{e}_i(t)| \le \frac{|\bar{e}_1(0)| + |\bar{e}_2(0)| + |\bar{e}_3(0)|}{\omega_{\min}^3} + \frac{M\bar{\gamma}}{\omega_{\min}^{4-i}} + \frac{M\bar{\eta}}{\omega_{\min}^{7-i}} \quad \forall t > T \tag{74}$$

where $\bar{\gamma} = \max\{\frac{1}{\bar{\beta}_3}, \frac{\bar{\beta}_1}{\bar{\beta}_3}, \frac{\bar{\beta}_2}{\bar{\beta}_3}\}, \bar{\eta} = \max\{\frac{1}{\bar{\beta}_3}, 1 + \frac{\bar{\beta}_1}{\bar{\beta}_3}, 1 + \frac{\bar{\beta}_2}{\bar{\beta}_3}\}$.■

Remark 3: Similar to AESO, the bound of estimation error depends on the initial estimation error, the upper bound of the second derivative of the lumped disturbance, and the observer gain. However, comparing (55) and (74), if the parameters β_1, β_2 and $\bar{\beta}_1, \bar{\beta}_2$ remain the same, and the parameter $\bar{\beta}_3$ is assigned to a specific value, the estimation accuracy is higher under the same working condition.

Theorem 4: Suppose that Assumption 2 is satisfied. The bounded stability of (70) under the control law (69) for any bounded $\dot{h}$ is guaranteed if the observer gain in (68) and controller gain in (69) are chosen such that $\bar{A}_{\bar{\varepsilon}}$ is the Hurwitz matrix and $k_{p1} > 0$.

Proof: Define the tracking error variable: $\delta = \omega^* - \omega$, then

$$\dot{\delta} = \dot{\omega}^* - \dot{\omega} = \dot{\omega}^* - bi_q^* - x_2. \tag{75}$$

According to (70) and (73), it can be obtained

$$\begin{aligned}\dot{\delta} &= \dot{\omega}^* - k_{p1}\delta + \begin{bmatrix}-k_{p1} & -1 & 0\end{bmatrix}\bar{\varepsilon}\\ &= \dot{\omega}^* - k_{p1}\delta + \begin{bmatrix}-k_{p1} & -\omega & 0\end{bmatrix}\bar{\varepsilon}\\ &= -k_{p1}\delta + \begin{bmatrix}-k_{p1} & -\omega & 0\end{bmatrix}\bar{\varepsilon}.\end{aligned} \tag{76}$$

TABLE IV
PARAMETERS OF PMSM

Descriptions	Parameters	Values
Stator Resistance	R_s	0.42 (Ω)
Stator Inductance	L_s	0.0035 (H)
Flux	ψ_f	0.168 (Wb)
Pole Pairs	p	4.0
Moment of inertia	J	0.113($g \cdot m^2$)
Rated torque	T_e	2.39 ($N \cdot m$)
Rated Speed	N_r	3000 (r/min)

The error equation (73) is rewritten as

$$\dot{\bar{\varepsilon}} = \omega A_{\bar{\varepsilon}}\varepsilon + B_{\bar{\varepsilon}}\frac{\dot{h}}{\omega^2} = \bar{A}_{\bar{\varepsilon}}\varepsilon + \bar{B}_{\bar{\varepsilon}}\dot{h}. \tag{77}$$

The tracking error equation and the estimation error equation can be obtained as

$$\begin{bmatrix}\dot{\delta}\\ \dot{\bar{\varepsilon}}\end{bmatrix} = \begin{bmatrix}-k_{p1} & \begin{bmatrix}-k_{p1} & -\omega & 0\end{bmatrix}\\ 0 & \bar{A}_{\bar{\varepsilon}}\end{bmatrix}\begin{bmatrix}\delta\\ \bar{\varepsilon}\end{bmatrix} + \begin{bmatrix}0\\ \bar{B}_{\bar{\varepsilon}}\end{bmatrix}\dot{h}. \tag{78}$$

Similar to the AESO, the stability of the closed-loop system based on AIESO is completed. ■

IV. Simulation Results

In order to verify the effectiveness of the proposed control strategy, the control strategy in Fig. 2 is verified by Matlab/Simulink software. The simulation parameters are the same as the actual platform parameters, as shown in Table IV. The simulation step size is 10 μs.

First, in order to demonstrate the effectiveness of the improved multistep FCS-MPCC based on sector proposed in the current loop, some simulations have been performed. The proposed control strategy is compared with the strategy in [19]. Except that the control strategy in current loop is different, the other condition keep same. The speed controller parameter is 0.2. The corresponding observer parameters are chosen as $\omega = 1500, \beta_1 = 1.5, \beta_2 = 0.1$. The simulation results are shown in Fig. 8. The reference speed is set to 800 r/min, PMSM starts at no load and the load torque $T_L = 5\text{N} \cdot \text{m}$ is applied to PMSM at $t = 0.15$ s. It can be seen that speed, current, and optimal voltage vector demonstrated under the two control strategy keep same, which is not only suitable for no-load but also for load operation. Especially the error of the optimal voltage vector number is 0, which further demonstrates the efficiency of the proposed strategy in this article.

Second, to further verify that AESO can deal with the contradiction between disturbance rejection and noise suppression, the composite control based on ESO and AESO are selected to compare. In order to ensure the fairness of comparison, an improved multistep FCS-MPCC based on sector is adopted in current loop. The controller parameter in speed loop is set to 0.2. The parameters of ESO are chosen as $\omega_{\min} = 800$,

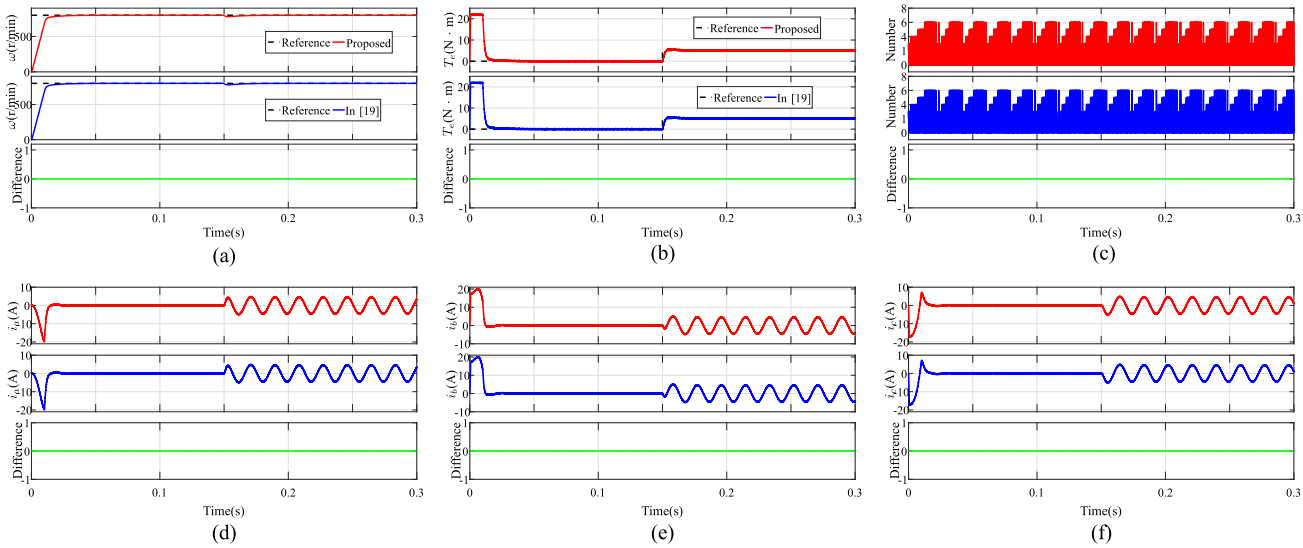

Fig. 8. Difference between the proposed current loop control strategy based on sector and the strategy in [19]. (a) Speed. (b) T_e. (c) Number. (d) i_a. (e) i_b. (f) i_c.

TABLE V
PERFORMANCE COMPARISON IN SIMULATIONS

	speed drop(r/min)	recovery time(s)
HGESO	20.7	0.0563
LGESO	27.5	0.1083
AESO	25	0.0888

$\omega_{\max} = 1500$, and the corresponding coefficients are set to $\beta_1 = 1.5, \beta_2 = 0.1, k = 0.5, m = 5$. The simulation results of high gain ESO(HGESO), low gain ESO(LGESO), and AESO are shown in Fig. 9. The speed, q-axis reference current, gain, and estimated value of the lumped disturbance x_2 are included. The corresponding speed is shown in Fig. 9(a). The load torque is suddenly added to PMSM at $t = 0.2$ s, and the load torque is 5 N $\cdot$ m. The corresponding speed drops and recovery times with the three observers in simulations are shown in Table V. It is easy to find that the disturbance rejection performance of the system with AESO is improved compared with the LGESO. The conclusion can also be drawn from Fig. 9(c). The adaptive gain of AESO increases when the load torque is suddenly changed. However, the adaptive gain keep lower gain when the system returns to the steady state again. According to the analysis of last section and the simulation result in Fig. 9(d), it can be accepted that the adaptive gain change will improve the disturbance rejection performance under load change and better suppress noise in steady state. In other words, the proposed AESO can adjust the gain in real time between low gain and high gain according to the estimation error, which can balance well the disturbance rejection performance and noise suppression.

Considering that the adaptive gain of AESO is adjusted based on estimation error and the disturbance will have a great impact on estimation error even gain of AESO, so the next task is to verify the impact of different disturbance on AESO. First, the

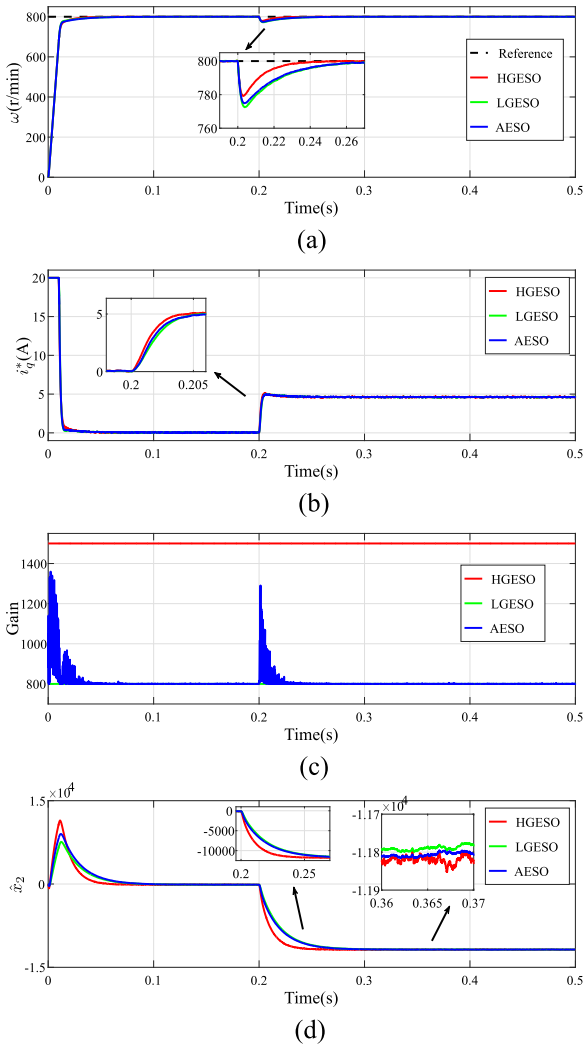

Fig. 9. Comparison of simulation results of low gain ESO, high gain ESO, and AESO. (a) Speed. (b) i_q^*. (c) Gain. (d) $\hat{x}_2$.

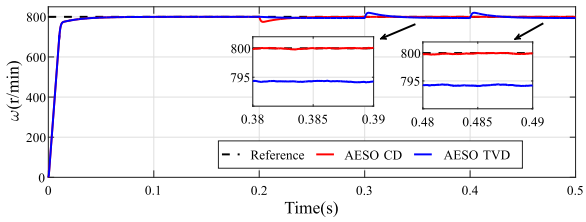

Fig. 10. Comparison of simulation results about speed of AESO subject to constant disturbance and time-varying disturbance.

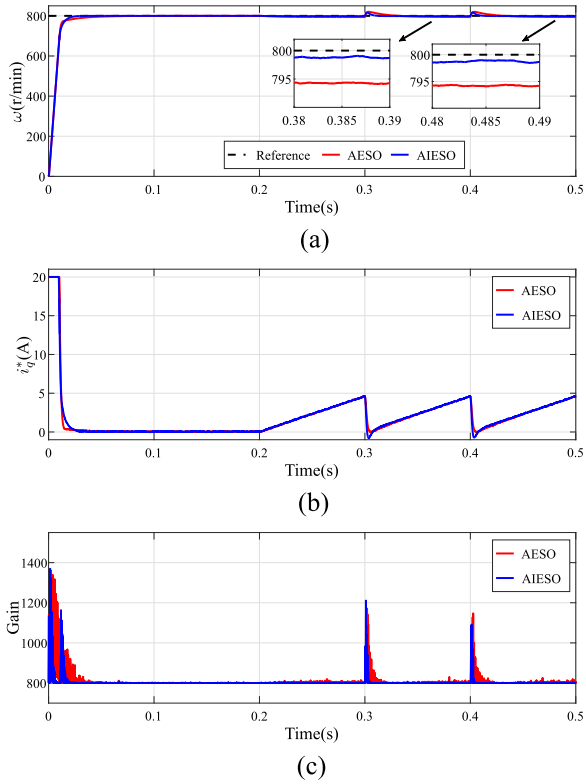

Fig. 11. Comparison of simulation results of AESO and AIESO subject to time-varying disturbance. (a) Speed. (b) i_q^*. (c) Gain.

PMSM is disturbed by constant load torque, the simulation result is shown in Fig. 10 (red curve). It can be seen that the speed of PMSM can quickly track the reference speed, and can also quickly recover to the steady-state value when disturbed by the sudden load torque. The blue curve in Fig. 10 represents the speed of PMSM subject to time-varying load torque. Except for the difference of disturbance type, other parameter conditions remain the same. It is obvious that the tracking accuracy for PMSM subject to time-varying load torque becomes poor. In other words, the speed can converge to the reference speed subject to constant load torque, there exists tracking error subject to time-varying load torque.

As seen in Fig. 10 (blue curve), the tracking error is about 5.6 r/min disturbed by time-varying load torque. To verify the improvement about tracking accuracy for the proposed AIESO, the same time-varying load torque is applied to compare. The parameter β_3 is selected to be $\beta_3 = 0.0005$. The simulation result is shown in Fig. 11. the tracking error is about 1.2 r/min

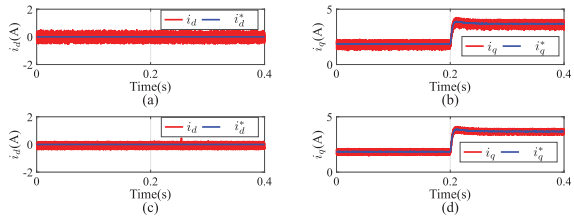

Fig. 12. Simulation results of the inductance parameter mismatch ($\bar{L}_s = 1.5L_s$). (a) i_d and i_d^*. (b) i_q and i_q^*. (c) i_d and i_d^* based on disturbance compensation. (d) i_q and i_q^* based on disturbance compensation.

in Fig. 11(a) (blue curve). Compared with AESO, the proposed AIESO can improve the tracking accuracy to some extent. The corresponding q-axis reference currents are shown in Fig. 11(b). Fig. 11(c) represents the gain of observer subject to time-varying load torque. When the system is disturbed by time-varying load torque, the gain will vary with the estimation error to balance the disturbance rejection and noise suppression.

Finally, in order to verify the proposed current loop control strategy with low parameter sensitivity based on sector and the improved multistep FCS-MPCC based on sector are simulated. The simulation results are shown in Figs. 12–17. The performance of the proposed method under load variation is verified, the load torque of PMSM changed from $2\ \mathrm{N{\cdot}m}$ to $4\ \mathrm{N\cdot m}$ at $t = 0.2$ s. Fig. 12 shows the current tracking curves with $\bar{L}_s = 1.5L_s$. Fig. 12(a) and (b), respectively, show the tracking curves of current i_d and i_q when inductance parameter does not match. It is easy to see that the current tracking accuracy is poor when inductance increases. In theory, when inductance parameter does not match, if the initial value of inductance is significantly different from the actual value, the estimated burden of the observer will be increased. In order to improve this problem, the state information of PMSM itself is used to make the estimated inductance value relatively closer to the real value, and the initial inductance value of the observer is updated with the estimated inductance parameter value, which will reduce the estimated burden of the observer. In addition, updating the prediction model will also improve the prediction performance of the system to some extent. The ESO is considered in this article to suppress the parameter mismatch. The parameter of the observer is chosen as $\omega_d = 250$. The corresponding simulation results are shown in Fig. 12(c) and (d), respectively, representing the current tracking curves after disturbance compensation. By comparing the simulation results, It is easy to see that the observer with the updated inductance value can well deal with tracking accuracy decline caused by the increase of inductance parameter. In order to compare the simulation results more accurately, integrated time absolute error (ITAE), and root mean squared error (RMSE) were used for quantitative analysis

$$\begin{cases} \mathrm{ITAE} = \int_0^{\mathrm{t}} \mathrm{t}\left|\mathrm{i_q} - \mathrm{i_q^*}\right| \mathrm{d}\tau \\ \mathrm{RMSE} = \sqrt{\int_0^t \frac{1}{t}\left(i_q - i_q^*\right)^2 d\tau}. \end{cases} \tag{79}$$

When parameter mismatch exists, the change of current i_q is easy to observe. For convenience, current i_q is taken as an example to evaluate the performance index. Table VII describes

TABLE VI
PERFORMANCE COMPARISON IN EXPERIMENTS

	speed drop(r/min)	recovery time(s)
HGESO	4.1	0.0665
LGESO	8.9	0.0745
AESO	8	0.0732

TABLE VII
PERFORMANCE INDEXES OF PARAMETER MISMATCHES IN SIMULATIONS

Cases	Current	ITAE	RMSE
	$i_q(0-0.4s)$	0.023	0.0051
$\bar{L}_s = 1.5L_s$	$i_q(0-0.4s)$	0.0178	0.0028
	Improvement	22.61%	45.10%
	$i_q(0-0.4s)$	0.0257	0.0062
$\bar{L}_s = 0.5L_s$	$i_q(0-0.4s)$	0.0179	0.0028
	Improvement	30.35%	54.84%
	$i_q(0-0.4s)$	0.0286	0.0070
$\bar{\psi}_f = 1.5\psi_f$	$i_q(0-0.4s)$	0.0167	0.0027
	Improvement	41.61%	61.43%
	$i_q(0-0.4s)$	0.0321	0.0085
$\bar{\psi}_f = 0.5\psi_f$	$i_q(0-0.4s)$	0.0203	0.0039
	Improvement	36.76%	54.12%
	$i_q(0-0.4s)$	0.01741	0.002686
$\bar{R}_s = 1.5R_s$	$i_q(0-0.4s)$	0.01740	0.002681
	Improvement	0.06%	0.19%
	$i_q(0-0.4s)$	0.0190	0.0032
$\bar{R}_s = 0.5R_s$	$i_q(0-0.4s)$	0.0185	0.0030
	Improvement	2.63%	6.25%

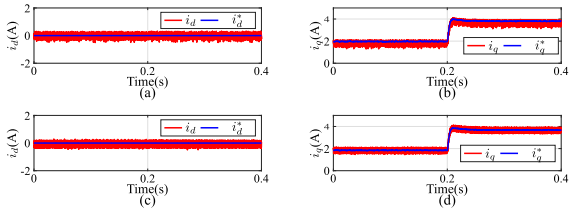

Fig. 13. Simulation results of the inductance parameter mismatch ($\bar{L}_s = 0.5L_s$). (a) i_d and i_d^*. (b) i_q and i_q^*. (c) i_d and i_d^* based on disturbance compensation. (d) i_q and i_q^* based on disturbance compensation.

the simulation performance indexes corresponding to Fig. 12. In order to make the quantitative analysis more reliable, the performance indexes in Table VII not only considers the steady-state situation when the inductance parameter does not match but also takes into account the dynamic process when the load torque changes. When the inductance parameter is increased, the ITAE and RMSE of current i_q are increased by 22.61% and 45.10% with $\bar{L}_s = 1.5\,L_s$, respectively. Similarly, when $\bar{L}_s = 0.5\,L_s$, the performance indexes of ITAE and RMSE are improved by 30.35% and 54.84%, respectively. The corresponding simulation diagram is shown in Fig. 13. Through the above simulation verification results and quantitative analysis results, it can be easily verified that the robustness of the system to the inductance

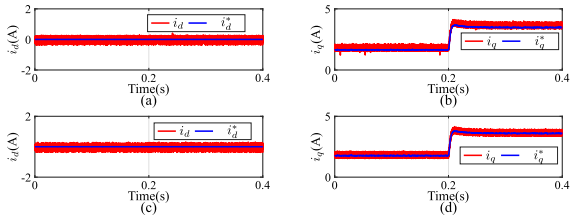

Fig. 14. Simulation results of the inductance parameter mismatch ($\bar{\psi}_f = 1.5\psi_f$). (a) i_d and i_d^*. (b) i_q and i_q^*. (c) i_d and i_d^* based on disturbance compensation. (d) i_q and i_q^* based on disturbance compensation.

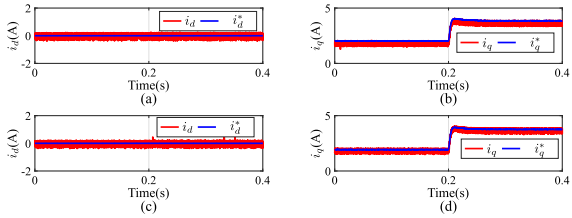

Fig. 15. Simulation results of the inductance parameter mismatch ($\bar{\psi}_f = 0.5\psi_f$). (a) i_d and i_d^*. (b) i_q and i_q^*. (c) i_d and i_d^* Based on disturbance compensation. (d) i_q and i_q^* Based on disturbance compensation.

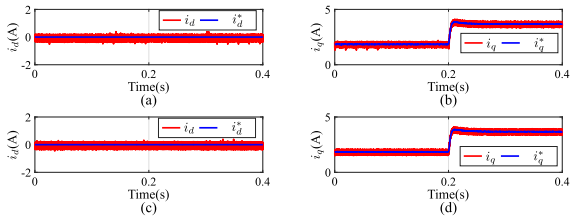

Fig. 16. Simulation results of the inductance parameter mismatch ($\bar{R}_s = 1.5R_s$). (a) i_d and i_d^*. (b) i_q and i_q^*. (c) i_d and i_d^* based on disturbance compensation. (d) i_q and i_q^* based on disturbance compensation.

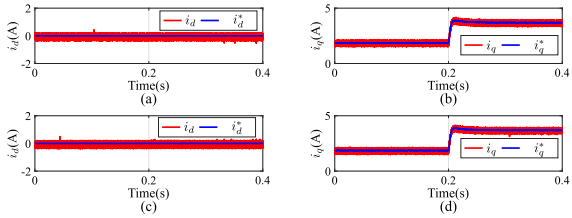

Fig. 17. Simulation results of the inductance parameter mismatch ($\bar{R}_s = 0.5R_s$). (a) i_d and i_d^*. (b) i_q and i_q^*. (c) i_d and i_d^* Based on disturbance compensation. (d) i_q and i_q^* based on disturbance compensation.

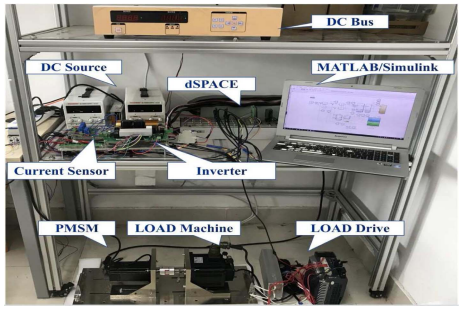

Fig. 18. Experimental platform.

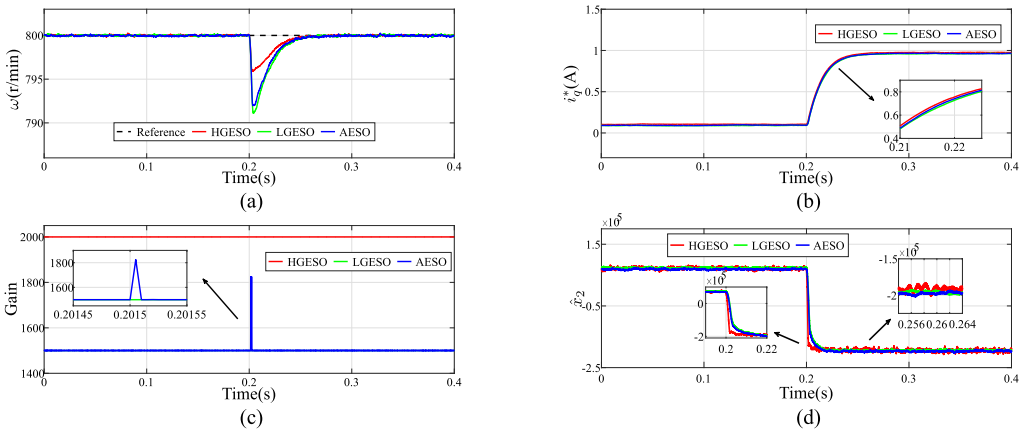

Fig. 19. Comparison of experimental results of low gain ESO, high gain ESO, and AESO. (a) Speed. (b) i_q^*. (c) Gain. (d) $\hat{x}_2$.

is improved by using the observer with the updated inductance value.

Then, in order to further verify whether the method of disturbance compensation can improve the robustness of the system to stator resistance and flux, the observer with updated inductance is still used for disturbance estimation and compensation. When the flux mismatch occurs, the corresponding simulation results are shown in Figs. 14 and 15. Fig. 14(a) and (b) represent the curves of current i_d and i_q with $\bar{\psi}_f = 1.5\psi_f$. Fig. 14(c) and (d) represent the curves of current i_d and i_q based on disturbance compensation. The disturbance compensation is accomplished by utilizing the observer with the updated initial inductance. The track curves of current with $\bar{\psi}_f = 0.5\psi_f$ are shown in Fig. 15. As can be seen from Figs. 14 and 15, the current tracking accuracy is improved after disturbance compensation by using the observer with the updated inductance. Similarly, when the stator resistance does not match, the curves of current i_d and i_q are shown in Figs. 16 and 17. The comparisons of performance indexes in simulations are shown in Table VII. It is easy to see that the system with disturbance compensation can well suppress the stator resistance mismatch and flux linkage mismatch.

V. Experimental Results

In order to validate the feasibility of the proposed control strategy, a experiment platform has been set up, as shown in Fig. 18. The platform is based on dSPACE 1103 controller board, the dc bus power supply is used to power the inverter and three phase current are measured for closed loop control by using the current sensors, the load motor is employed to provide load torque for the controlled PMSM. The parameters of the PMSM are shown in Table IV.

The experimental results of HGESO, LGESO, AESO, and AIESO are discussed in Figs. 19–21. The controller parameter in speed loop is set to 0.05. The parameters of ESO are chosen as $\omega_{\min} = 1500$, $\omega_{\max} = 2000$, the corresponding coefficients are set to $\beta_1 = 1.5, \beta_2 = 0.1$, and the other coefficients are $k = 4.6 \times 10^{-3}, m = 10$. The reference speed is 800 r/min. The load torque is 1 N · m. Fig. 19 shows the speed, q-axis reference current gain and estimated value of the lumped disturbance x_2

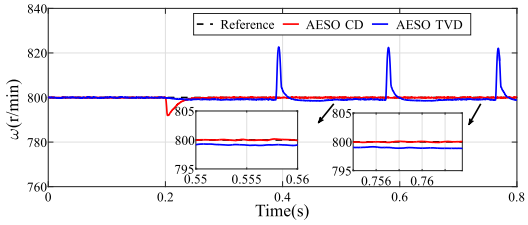

Fig. 20. Comparison of experimental results about speed of AESO subject to constant disturbance and time-varying disturbance.

corresponding to HGESO, LGESO, and AESO. When the load torque of PMSM changes, the corresponding speed drops and recovery times with the three observers in experiments are shown in Table VI. Similar to the simulation results, the speed decrease of the composite control strategy based on AESO is between HGESO and LGESO when the load torque is added to PMSM. That is to say, compared with LGESO, the disturbance rejection performance of the system with AESO has been improved. The adaptive gain corresponding to AESO also show the similar conclusion in Fig. 19(c). And it can be obtained that the noise amplification caused by high gain is improved to some extent according to the Fig. 19(d).

When PMSM is subject to the constant load torque and time-varying load torque, respectively, the experimental result is shown in Fig. 20. PMSM is in steady-state operation at the beginning. When subjected to the constant load torque, PMSM can return to reference speed again. However, when the time-varying load torque is applied to PMSM, the tracking error will occur, which means that the tracking accuracy for the closed-loop system becomes poor. In order to deal with this problem, the experimental result of the composite control strategy based on AIESO is shown in Fig. 21.

In order to verify whether the integral term will improve tracking error, the other parameters are kept same except for the parameter β_3. The parameter β_3 is selected to be $\beta_3 = 3.33 \times 10^{-4}$. It can be seen that the tracking accuracy of the composite control strategy based on AIESO is higher than that of the composite control strategy based on AESO in Fig. 21(a). The q-axis reference currents are also demonstrated in Fig. 21(b).

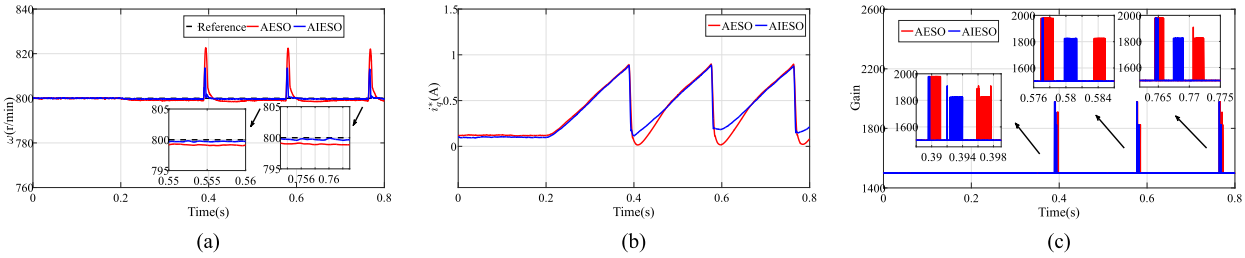

Fig. 21. Comparison of experimental results of AESO and AIESO subject to time-varying disturbance. (a) Speed. (b) i_q^*. (c) Gain.

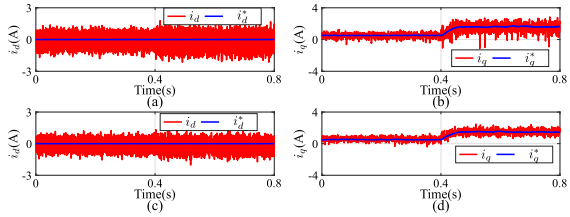

Fig. 22. Experimental results of the inductance parameter mismatch ($\bar{L}_s = 1.5L_s$). (a) i_d and i_d^*. (b) i_q and i_q^*. (c) i_d and i_d^* based on disturbance compensation. (d) i_q and i_q^* based on disturbance compensation.

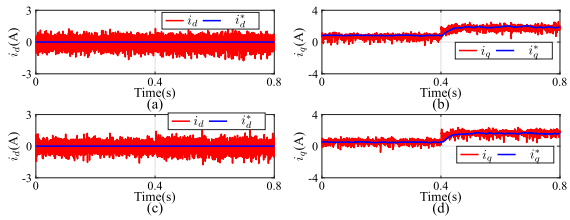

Fig. 23. Experimental results of the inductance parameter mismatch ($\bar{L}_s = 0.5L_s$). (a) i_d and i_d^*. (b) i_q and i_q^*. (c) i_d and i_d^* based on disturbance compensation. (d) i_q and i_q^* based on disturbance compensation.

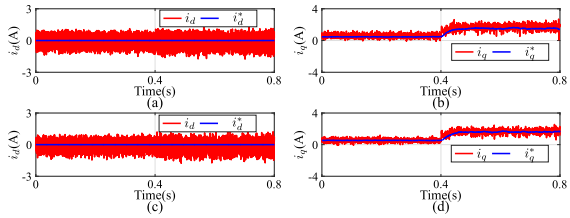

Fig. 24. Experimental results of the flux linkage mismatch($\bar{\psi}_f = 1.5\psi_f$). (a) i_d and i_d^*. (b) i_q and i_q^*. (c) i_d and i_d^* based on disturbance compensation. (d) i_q and i_q^* based on disturbance compensation.

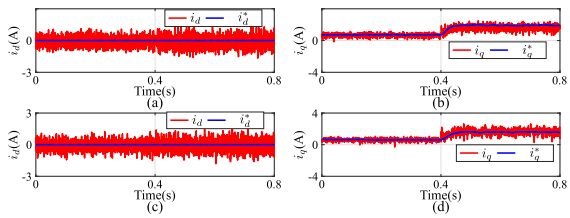

Fig. 25. Experimental results of the flux linkage mismatch ($\bar{\psi}_f = 0.5\psi_f$). (a) i_d and i_d^*. (b) i_q and i_q^*. (c) i_d and i_d^* based on disturbance compensation. (d) i_q and i_q^* based on disturbance compensation.

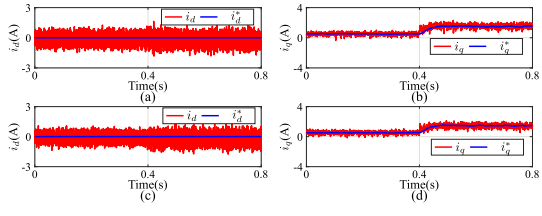

Fig. 26. Experimental results of the stator resistance mismatch ($\bar{R}_s = 1.5R_s$). (a) i_d and i_d^*. (b) i_q and i_q^*. (c) i_d and i_d^* based on disturbance compensation. (d) i_q and i_q^* based on disturbance compensation.

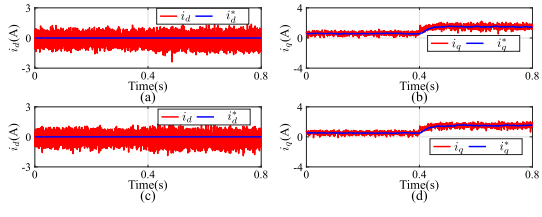

Fig. 27. Experimental results of the stator resistance mismatch ($\bar{R}_s = 0.5R_s$). (a) i_d and i_d^*. (b) i_q and i_q^*. (c) i_d and i_d^* based on disturbance compensation. (d) i_q and i_q^* based on disturbance compensation.

TABLE VIII
PERFORMANCE INDEXES OF PARAMETER MISMATCHES IN EXPERIMENTS

Cases	Current	ITAE	RMSE
	$i_q(0-0.8s)$	0.1846	0.1014
$\bar{L}_s = 1.5L_s$	$i_q(0-0.8s)$	0.1283	0.0413
	Improvement	30.50%	59.27%
	$i_q(0-0.8s)$	0.1512	0.0611
$\bar{L}_s = 0.5L_s$	$i_q(0-0.8s)$	0.1395	0.0512
	Improvement	7.74%	16.20%
	$i_q(0-0.8s)$	0.1642	0.0674
$\bar{\psi}_f = 1.5\psi_f$	$i_q(0-0.8s)$	0.1202	0.0379
	Improvement	26.80%	43.77%
	$i_q(0-0.8s)$	0.1532	0.0642
$\bar{\psi}_f = 0.5\psi_f$	$i_q(0-0.8s)$	0.1235	0.0428
	Improvement	19.39%	33.33%
	$i_q(0-0.8s)$	0.1074	0.0316
$\bar{R}_s = 1.5R_s$	$i_q(0-0.8s)$	0.1056	0.0285
	Improvement	1.68%	9.81%
	$i_q(0-0.8s)$	0.1005	0.0267
$\bar{R}_s = 0.5R_s$	$i_q(0-0.8s)$	0.0916	0.0227
	Improvement	8.86%	14.98%

No matter strategy based on AESO or strategy based on AIESO, when the system is disturbed by time-varying load torque, their adaptive gain will change accordingly in Fig. 21(c).

Similar to simulation, it is verified whether the observer with updated inductance has disturbance compensation effect on parameter mismatches (including load torque variation). The parameter of observer are chosen as $\omega_d = 500$. The corresponding experimental results are shown in Figs. 22–27. And the comparisons of performance indexes in experiments are shown in Table VIII. It can be easily concluded that the observer with updated inductance parameter can improve the tracking accuracy of current when the parameters do not match. That is to say, the robustness of the system to motor parameters is improved to some extent.

VI. Conclusion

In this article, an improved multistep FCS-MPCC based on AIESO has been proposed for PMSM. First, in order to further reduce the computational burden of the multistep FCS-MPCC in [19], an improved multistep FCS-MPCC based on sector has been studied. The control performance of the proposed method is consistent with that of [19], but less computation. Second, in order to balance the disturbance rejection performance of system and noise suppression. AESO has been proposed to solve this problem. However AESO will lead to poor steady-state tracking accuracy because of the time-varying disturbance. Thus, AIESO has been proposed to improve the steady-state tracking accuracy, which not only balances disturbance rejection performance of system and noise suppression but also improves steady-state tracking accuracy. Third, in order to suppress the impact of parameter mismatches, the inductance parameter estimation method and disturbance compensation mechanism are applied to the current loop to improve the robustness of the system to motor parameters. Finally, simulation and experimental results have shown the effectiveness of the improved multistep FCS-MPCC with low parameter sensitivity based on AIESO proposed in this article.

References

[1] H. Liu and S. Li, "Speed control for PMSM servo system using predictive functional control and extended state observer," *IEEE Trans. Ind. Electron.*, vol. 59, no. 2, pp. 1171–1183, Feb. 2012.

[2] L. He, F. Wang, J. Wang, and J. Rodrlguez, "Zynq implemented luenberger disturbance observer based predictive control scheme for PMSM drives," *IEEE Trans. Power Electron.*, vol. 35, no. 2, pp. 1770–1778, Feb. 2020.

[3] X. Li, Q. Yang, W. Tian, P. Karamanakos, and R. Kennel, "A dual reference frame multistep direct model predictive current control with a disturbance observer for SPMSM drives," *IEEE Trans. Power Electron.*, vol. 37, no. 3, pp. 2857–2869, Mar. 2022.

[4] B. Yu, W. Song, Y. Guo, and M. S. R. Saeed, "A finite control set model predictive control for five-phase PMSMs with improved DC-Link utilization," *IEEE Trans. Power Electron.*, vol. 37, no. 3, pp. 3297–3307, Mar. 2022.

[5] S. Vazquez, J. Rodriguez, M. Rivera, L. G. Franquelo, and M. Norambuena, "Model predictive control for power converters and drives: Advances and trends," *IEEE Trans. Ind. Electron.*, vol. 64, no. 2, pp. 935–947, Feb. 2017.

[6] A. Favato, P. G. Carlet, F. Toso, R. Torchio, and S. Bolognani, "Integral model predictive current control for synchronous motor drives," *IEEE Trans. Power Electron.*, vol. 36, no. 11, pp. 13293–13303, Nov. 2021.

[7] A. A. Ahmed, B. K. Koh, and Y. I. Lee, "A comparison of finite control set and continuous control set model predictive control schemes for speed control of induction motors," *IEEE Trans. Ind. Inform.*, vol. 14, no. 4, pp. 1334–1346, Apr. 2018.

[8] M. Siami, D. A. Khaburi, and J. Rodriguez, "Simplified finite control set-model predictive control for matrix converter-fed PMSM drives," *IEEE Trans. Power Electron.*, vol. 33, no. 3, pp. 2438–2446, Mar. 2018.

[9] P. Karamanakos and T. Geyer, "Guidelines for the design of finite control set model predictive controllers," *IEEE Trans. Power Electron.*, vol. 35, no. 7, pp. 7434–7450, Jul. 2020.

[10] F. Wang, G. Lin, and Y. He, "Passivity-based model predictive control of three-level inverter-fed induction motor," *IEEE Trans. Power Electron.*, vol. 36, no. 2, pp. 1984–1993, Feb. 2021.

[11] T. Geyer and D. E. Quevedo, "Multistep finite control set model predictive control for power electronics," *IEEE Trans. Power Electron.*, vol. 29, no. 12, pp. 6836–6846, Dec. 2014.

[12] T. Geyer and D. E. Quevedo, "Performance of multistep finite control set model predictive control for power electronics," *IEEE Trans. Power Electron.*, vol. 30, no. 3, pp. 1633–1644, Mar. 2015.

[13] X. Zhang, K. Yan, and M. Cheng, "Two-stage series model predictive torque control for PMSM drives," *IEEE Trans. Power Electron.*, vol. 36, no. 11, pp. 12910–12918, Nov. 2021.

[14] C. Xia, T. Liu, T. Shi, and Z. Song, "A simplified finite-control-set model-predictive control for power converters," *IEEE Trans. Ind. Inform.*, vol. 10, no. 2, pp. 991–1002, May 2014.

[15] W. Xie et al., "Finite-control-set model predictive torque control with a deadbeat solution for PMSM drives," *IEEE Trans. Ind. Electron.*, vol. 62, no. 9, pp. 5402–5410, Sep. 2015.

[16] Y. Zhang, H. Yang, and X. Wei, "Model predictive control of permanent magnet synchronous motors based on fast vector selection," *Trans. China Electrotechnical Soc.*, vol. 31, no. 6, pp. 66–73, Mar. 2016 (in Chinese).

[17] P. Cortes, J. Rodriguez, S. Vazquez, and L. G. Franquelo, "Predictive control of a three-phase UPS inverter using two steps prediction horizon," in *Proc. IEEE Int. Conf. Ind. Technol.*, 2010, pp. 1283–1288.

[18] B. Q. Van Ngo, P. Rodriguez-Ayerbe, and S. Olaru, "Model predictive control with two-step horizon for three-level neutral-point clamped inverter," in *Proc. Int. Conf. Process Control*, 2015, pp. 215–220.

[19] J. Wang, H. Yang, Y. Liu, and J. Rodriguez, "Low-cost multistep FCS-MPCC for PMSM drives using a DC link single current sensor," *IEEE Trans. Power Electron.*, vol. 37, no. 9, pp. 11034–11044, Sep. 2022.

[20] J. Han, "From PID to active disturbance rejection control," *IEEE Trans. Ind. Electron.*, vol. 56, no. 3, pp. 900–906, Mar. 2009.

[21] Z. Gao, "Scaling and bandwidth-parameterization based controller tuning," in *Proc. Amer. Control Conf.*, 2003, pp. 4989–4996.

[22] S. Li, J. Yang, W. -H. Chen, and X. Chen, "Generalized extended state observer based control for systems with mismatched uncertainties," *IEEE Trans. Ind. Electron.*, vol. 59, no. 12, pp. 4792–4802, Dec. 2012.

[23] Y. Zhang, J. Jin, and L. Huang, "Model-free predictive current control of PMSM drives based on extended state observer using ultralocal model," *IEEE Trans. Ind. Electron.*, vol. 68, no. 2, pp. 993–1003, Feb. 2021.

[24] Y. Zhang, T. Jiang, and J. Jiao, "Model-free predictive current control of DFIG based on an extended state observer under unbalanced and distorted grid," *IEEE Trans. Power Electron.*, vol. 35, no. 8, pp. 8130–8139, Aug. 2020.

[25] J. Song, Z. Gan, and J. Hang, "Study of active disturbance rejection controller on filtering," *Control Decis.*, vol. 18, no. 1, pp. 11034–11044, Jan. 2003 (in Chinese).

[26] F. Lin, H. Sun, Q. Zheng, and Y. Xia, "Novel extended state observer for uncertain system with measurement noise," *Control Theory Appl.*, vol. 22, no. 6, pp. 995–998, Dec. 2005 (in Chinese).

[27] Y. Wang, Y. Yao, and K. Ma, "A new type extended state observer for system with measurement noise," in *Proc. IEEE Int. Conf. Autom. Logistics*, Qingdao, China, 2008, pp. 1745–1749.

[28] H. Sun, R. Madonski, S. Li, Y. Zhang, and W. Xue, "Composite control design for systems with uncertainties and noise using combined extended state observer and kalman filter," *IEEE Trans. Ind. Electron.*, vol. 69, no. 4, pp. 4119–4128, Apr. 2022.

[29] K. Lakomy et al., "Active disturbance rejection control design with suppression of sensor noise effects in application to DC-DC buck power converter," *IEEE Trans. Ind. Electron.*, vol. 69, no. 1, pp. 816–824, Jan. 2022.

[30] S. Ahmad and A. Ali, "On active disturbance rejection control in presence of measurement noise," *IEEE Trans. Ind. Electron.*, vol. 69, no. 11, pp. 11600–11610, Nov. 2022.

[31] X. Zhang, L. Zhang, and Y. Zhang, "Model predictive current control for PMSM drives with parameter robustness improvement," *IEEE Trans. Power Electron.*, vol. 34, no. 2, pp. 1645–1657, Feb. 2019.

[32] W. Wang, X. Xiao, and Y. Ding, "An adaptive incremental predictive current control method of PMSM," in *Proc. IEEE 15th Eur. Conf. Power Electron. Appl.*, 2013, pp. 1–8.
[33] L. Niu, M. Yang, K. Liu, and D. Xu, "A predictive current control scheme for permanent magnet synchronous motors," in *Proc. Chin. Soc. Elect. Eng.*, 2012, vol. 32, no. 6, pp. 132–135.
[34] X. Yu, D. Ke, Z. Zhang, F. Wang, and J. Rodrlguez, "Robust exploration based finite control set predictive current control for SPMSM drives under influence of measurement error," *IEEE Trans. Energy Convers.*, early access, Feb. 27, 2023, doi: 10.1109/TEC.2023.3249211.
[35] X. Zhang, B. Hou, and Y. Mei, "Deadbeat predictive current control of permanent-magnet synchronous motors with stator current and disturbance observer," *IEEE Trans. Power Electron.*, vol. 32, no. 5, pp. 3818–3834, May 2017.
[36] C. Lin, T. Liu, J. Yu, L. Fu, and C. Hsiao, "Model-free predictive current control for interior permanent-magnet synchronous motor drives based on current difference detection technique," *IEEE Trans. Ind. Electron.*, vol. 61, no. 2, pp. 667–681, Feb. 2014.

Junxiao Wang (Senior Member, IEEE) received the B.S. degree in automation and the M.S. degree in control theory and control engineering from the School of Information Engineering, Henan University of Science and Technology, Luoyang, China, in 2008 and 2011, respectively, and the Ph.D. degree in control theory and control engineering from the School of Automation, Southeast University, Nanjing, China, in 2017.

From 2015 to 2016, he was a visiting Ph.D. student with the Institute for Electrical Drive Systems and Power Electronics, Technical University of Munich, Munich, Germany. He is currently with the College of Information Engineering, Zhejiang University of Technology, Hangzhou, China. His research interests include advanced control theory and its application to power electronics and motion control systems.

Dr. Wang was the recipient of 2017 IET Premium Award for best paper in IET Control Theory & Applications (First Author). He serves as an Associate Editor for *International Journal of Electronics and Letters*.

Yibin Liu was born in Henan Province, China, in 1995. He received the B.S. degree in automation from Hubei University of Technology, Wuhan, China in 2017. He is currently working toward the M.S. degree in control science and engineering with the College of Information Engineering, Zhejiang University of Technology, Hangzhou, China.

His research interests include model predictive control for electrical drives.

Jun Yang (Fellow, IEEE) received the B.Sc. degree in automation from the Department of Automatic Control, Northeastern University, Shenyang, China, in 2006, and the Ph.D. degree in control theory and control engineering from the School of Automation, Southeast University, Nanjing, China in 2011.

He joined the Department of Aeronautical and Automotive Engineering, Loughborough University, Loughborough, U.K., from 2020, as a Senior Lecturer. His research interests include disturbance observer, motion control, visual servoing, nonlinear control, and autonomous systems.

Dr. Yang is a Fellow of Institution of Engineering and Technology and American Institute of Aeronautics and Astronautics. He was the recipient of the EPSRC New Investigator Award. He serves as Associate Editor or Technical Editor for IEEE TRANSACTIONS ON INDUSTRIAL ELECTRONICS, IEEE-ASME TRANSACTIONS ON MECHATRONICS, and IEEE OPEN JOURNAL OF INDUSTRIAL ELECTRONICS SOCIETY.

Fengxiang Wang (Senior Member, IEEE) was born in Jiujiang, China, in 1982. He received the B.S. degree in electronic engineering and the M.S. degree in automation from Nanchang Hangkong University, Nanchang, China, in 2005 and 2008, respectively, and the Ph.D. degree in electrical engineering from the Institute for Electrical Drive Systems and Power Electronics, Technische Universitaet Muenchen, Munich, Germany, in 2014.

He is currently working as a Full Professor and deputy Director of Quanzhou Institute of Equipment Manufacturing, Haixi Institutes, Chinese Academy of Sciences, Beijing, China. His research interests include predictive control and sensorless control for electrical drives and power electronics.

Dr. Wang is a Fellow of IET. He is an Associate Editor for IEEE TRANSACTIONS ON INDUSTRIAL ELECTRONICS and IEEE TRANSACTIONS ON ENERGY CONVERSION. As General Chair, he organized the IEEE 5th International Symposium on Predictive Control of Electrical Drives and Power Electronics.

José Rodríguez (Life Fellow, IEEE) received the engineer degree in electrical engineering from the Universidad Tecnica Federico Santa Maria, Valparaiso, Chile, in 1977, and the Dr.-Ing. degree in electrical engineering from the University of Erlangen, Erlangen, Germany, in 1985.

He has been with the Department of Electronics Engineering, Universidad Tecnica Federico Santa Maria, since 1977, where he was full Professor and President. Since 2015, he has been the President of Universidad Andres Bello, Santiago, Chile. He has coauthored two books, several book chapters, and more than 400 journal and conference papers. His research interests include multilevel inverters, new converter topologies, control of power converters, and adjustable-speed drives.

Dr. Rodríguez is member of the Chilean Academy of Engineering. He was the recipient of a number of best paper awards from journals of the IEEE. He was the recipient of the National Award of Applied Sciences and Technology from the government of Chile, in 2014, and the Eugene Mittelmann Award from the Industrial Electronics Society of the IEEE, in 2015.